Published for SISSA by Springer

Received: December 3, 2015
Accepted: December 23, 2015
Published: January 13, 2016

Strong tW scattering at the LHC

Jeff Asaf Dror,[a] **Marco Farina,**[a,b] **Ennio Salvioni**[c] **and Javi Serra**[d,e]

[a] *LEPP, Department of Physics, Cornell University, Newman Laboratory, Ithaca, NY, 14853 U.S.A.*

[b] *New High Energy Theory Center, Department of Physics, Rutgers University, 136 Frelinghuisen Road, Piscataway, NJ, 08854 U.S.A.*

[c] *Department of Physics, University of California, Davis, One Shields Avenue, Davis, CA, 95616 U.S.A.*

[d] *Dipartimento di Fisica e Astronomia, Università di Padova and INFN, Sezione di Padova, Via Marzolo 8, Padova, I-35131 Italy*

[e] *Theory Department, CERN, Geneva 23, CH-1211 Switzerland*

E-mail: ajd268@cornell.edu, farina@physics.rutgers.edu, esalvioni@ucdavis.edu, javier.serra.mari@cern.ch

Abstract: Deviations of the top electroweak couplings from their Standard Model values imply that certain amplitudes for the scattering of third generation fermions and longitudinally polarized vector bosons or Higgses diverge quadratically with momenta. This high-energy growth is a genuine signal of models where the top quark is strongly coupled to the sector responsible for electroweak symmetry breaking. We propose to profit from the high energies accessible at the LHC to enhance the sensitivity to non-standard top-Z couplings, which are currently very weakly constrained. To demonstrate the effectiveness of the approach, we perform a detailed analysis of $tW \to tW$ scattering, which can be probed at the LHC via $pp \to t\bar{t}Wj$. By recasting a CMS analysis at 8 TeV, we derive the strongest direct bounds to date on the Ztt couplings. We also design a dedicated search at 13 TeV that exploits the distinctive features of the $t\bar{t}Wj$ signal. Finally, we present other scattering processes in the same class that could provide further tests of the top-Higgs sector.

Keywords: Beyond Standard Model, Heavy Quark Physics

ArXiv ePrint: 1511.03674

Open Access, © The Authors.
Article funded by SCOAP[3].

doi:10.1007/JHEP01(2016)071

JHEP01(2016)071

Contents

1 Introduction **1**

2 Parameterization of top and Higgs couplings **3**

3 $tW \to tW$ scattering as case study **7**

4 $t\bar{t}W$ analysis **13**
- 4.1 8 TeV bounds 14
- 4.2 Background simulation 17
- 4.3 13 TeV analysis 19
  - 4.3.1 $4j$ analysis 20
  - 4.3.2 $3j$ analysis 22
- 4.4 Perturbative unitarity of the hard scattering process 23

5 Other processes **25**
- 5.1 $tZ \to th$ 25
- 5.2 $bW \to th$ 26
- 5.3 $bW \to tZ$ 27
- 5.4 $tZ \to tZ$ 27
- 5.5 $t\bar{t} \to hh$ 28

6 Conclusions **29**

A Electroweak chiral Lagrangian **30**

B Current and projected $t\bar{t}Z$ constraints **31**
- B.1 8 TeV $t\bar{t}Z$ bound 31
- B.2 13 TeV $t\bar{t}Z$ projection 32

C Fake lepton simulation **32**

JHEP01(2016)071

1 Introduction

The large center of mass energies accessible at the LHC make it the optimal machine to explore the electroweak scale. This has already been confirmed by the discovery of the Higgs boson [1, 2], which represents the main achievement of Run-1 and a major step forward for particle physics. Another important example of the power of the LHC is the large rate for production of the top quark, the particle in the Standard Model (SM) with the largest coupling to the Higgs field. However, our knowledge of the properties of both

the Higgs and the top is still relatively poor. Since these two particles play a central role in theories beyond the SM (BSM) that provide a deeper understanding of electroweak symmetry breaking (EWSB), the program of Higgs and top coupling measurements is one of the priorities of LHC Run-2. The importance of this task is reinforced by the thus far lack of evidence for direct production of BSM particles, which may suggest that probes of the Higgs and top sectors are our best opportunity to gain new insights into the mechanism of EWSB.

The complicated hadronic environment at the LHC, however, does not facilitate the desired experimental precision. For example, experimental tests of the Ztt and htt couplings are very challenging: the conventional strategy consists in measuring the cross section for $t\bar{t}Z$ and $t\bar{t}h$ production, respectively. These processes have a relatively high mass threshold and thus suppressed production rates at the LHC. This leads to very loose constraints on the top couplings, currently well above the SM expectations. On the other hand, projections indicate that the htt coupling could be measured with 15% accuracy by the end of Run-2 [3], whereas the expected precision on Ztt is worse, and deviations as large as 50–100% will not be excluded [4–6].

One is then prompted to ask if there exists another avenue to probe the properties of the Higgs and the top. An answer has been given already for the couplings of the Higgs boson: if the Higgs couplings to the electroweak gauge bosons depart from the SM predictions, the amplitudes for the scattering of the longitudinally polarized $V = W, Z$ and Higgs h undergo a rapid growth with momentum above the weak scale $v \simeq 246\,\text{GeV}$. The prime example is $VV \to VV$ scattering, which grows with momenta as p^2/v^2 whenever the hVV coupling deviates from the SM [7], while the process $VV \to hh$ provides complementary information [8]. Such growth with energy is a distinctive feature of models where the Higgs emerges as a pseudo-Goldstone boson from a strongly-coupled sector [9–11]. In this class of theories, the high-energy enhancement can be accessed without directly producing the BSM resonances, which are strongly coupled to the Higgs but heavy. In complete analogy, the electroweak couplings of the top could be probed in the high-energy scattering of third generation fermions and longitudinal gauge bosons or Higgses. A growth with energy of the associated amplitudes would constitute a genuine signal of the strong coupling of the top to the BSM sector [12–14]. It was observed a long time ago [15] that a deviation from the SM in the $h\psi\psi$ coupling (with ψ a SM fermion) leads to a growth proportional to $m_\psi p/v^2$ of scattering amplitudes such as $\psi\bar{\psi} \to VV$, and this observation was recently exploited in refs. [16, 17] to constrain the htt coupling at the LHC, via the scattering $bW \to th$ in the $pp \to thj$ process [18].

In this paper we perform a general analysis of the scattering of tops (and bottoms) with the longitudinal W, Z or the Higgs. We point out that in the presence of deviations in the Ztt couplings, certain amplitudes grow like p^2/v^2 (rather than $m_t p/v^2$), leading to an enhanced sensitivity at the LHC. The $tW \to tW$ amplitude is singled out as the most promising one, because deviations in either the Zt_Lt_L or Zt_Rt_R couplings lead to the strong high-energy behavior. Furthermore, the corresponding LHC process is $pp \to t\bar{t}Wj$, which gives a clean same-sign leptons signature. We perform a detailed analysis of this signal, exploiting the information contained in the CMS 8 TeV search for $t\bar{t}W$ of ref. [19],

JHEP01(2016)071

and show that it gives stronger constraints than the conventional strategy relying on $pp \to t\bar{t}Z$. Motivated by the effectiveness of our approach at 8 TeV, we then design a specific search for Run-2 at 13 TeV, which we hope will help in refining the physics analyses of the experimental collaborations.

We also interpret our analysis in terms of non-standard top couplings arising from dimension-6 (dim-6) operators added to the SM Lagrangian, and show that competitive bounds are obtained in this case too. In this framework, correlations arise between the couplings of the top to the Z and to the W. Moreover, deviations in these couplings imply a p^2/v^2 growth not only of the tV scattering amplitudes, but also of those involving the Higgs, such as $bW \to th$ [20]. Thus, the interest of our approach does not end here: we discuss several other amplitudes that we believe to be promising in probing the top electroweak couplings, and that warrant further work to assess the expected sensitivity at the LHC.

Our paper is organized as follows. In section 2 we introduce our parameterization of couplings in the top-Higgs sector, discuss the current experimental constraints and outline the generic aspects of the scattering of third generation fermions with electroweak vector bosons and Higgses. Section 3 contains the discussion of the $tW \to tW$ scattering and the associated LHC process $pp \to t\bar{t}Wj$, as well as the main results of our paper. Section 4 contains the technical details of our collider analysis of $t\bar{t}Wj$, as well as the description of the method we use to obtain constraints on the top-Z interactions. This section can be omitted by the reader interested only in the results, who can move on to section 5, where we discuss other scattering processes that may provide additional information on the top-Higgs sector. Finally, section 6 contains our conclusions. Three appendices complete the paper: appendix A presents the electroweak chiral Lagrangian for the top sector, appendix B summarizes the current and projected constraints on top-Z couplings obtained from $pp \to t\bar{t}Z$, and appendix C details the procedure we adopt to simulate 'fake' leptons, which constitute one of the main backgrounds to our $t\bar{t}Wj$ signal.

2 Parameterization of top and Higgs couplings

In this section we introduce the general parameterization of the couplings relevant for the scattering of top quarks with the electroweak vector bosons W and Z and with Higgs boson h. The interactions of the top (and bottom) are encoded in the phenomenological Lagrangian

$$\begin{aligned}\mathcal{L}_t = {} & Z_\mu \bar{t}\gamma^\mu \left[c_L(h) g_{Zt_Lt_L} P_L + c_R(h) g_{Zt_Rt_R} P_R\right] t + Z_\mu \bar{b}\gamma^\mu \left[c_{L^b}(h) g_{Zb_Lb_L} P_L + c_{R^b}(h) g_{Zb_Rb_R} P_R\right] b \\ & + g_{Wt_Lb_L} W^+_\mu \bar{t}\gamma^\mu \left[c_{LL}(h) P_L + c_{RR}(h) P_R\right] b + \text{h.c.} - c_t(h) \frac{m_t}{v} h\, \bar{t}t\,, \end{aligned} \tag{2.1}$$

where $P_{L,R}$ are the left (L) and right (R) chiral projectors, $g_{Wt_Lb_L} = g/\sqrt{2}$, $g_{Zf_Rf_R} = -(gs_w^2/c_w)Q_f$, $g_{Zf_Lf_L} = (g/c_w)(T^3_{L,f} - Q_f s_w^2)$ are the SM gauge couplings, and $v \simeq 246$ GeV. We have defined the coefficients above as linear functions of h,

$$c_i(h) \equiv c_i + 2c_i^h \frac{h}{v}\,, \tag{2.2}$$

JHEP01(2016)071

$(i = \{L, R, L^b, R^b, LL, RR, t\})$, such that they also encode BSM couplings of the Higgs. We will also describe the hVV and Higgs cubic couplings with the Lagrangian

$$\mathcal{L}_h = c_V \frac{m_W^2}{v} h \left(2W_\mu^+ W^{-\mu} + \frac{1}{c_w^2} Z_\mu Z^\mu \right) - c_3 \frac{m_h^2}{2v} h^3 \,. \tag{2.3}$$

The coefficients c_i, c_i^h, c_V and c_3 parameterize the relevant couplings of the third generation fermions, W, Z, and h. The SM Lagrangian is reproduced for

$$c_L = c_R = c_{L^b} = c_{R^b} = c_{LL} = c_t = c_V = c_3 = 1 \,, \qquad c_{RR} = 0 \,, \qquad c_i^h = 0 \,. \tag{2.4}$$

We now wish to comment on the rationale behind our parameterization. As explained in appendix A, the phenomenological Lagrangian in eqs. (2.1) and (2.3) can be regarded as the unitary gauge version of the leading set of operators, in an expansion in derivatives, of the electroweak chiral Lagrangian [21, 22] (for recent thorough discussions of the electroweak chiral Lagrangian, see refs. [8, 23]). We are neglecting, for instance, BSM chirality-flipping interactions of the fermions with W and Z, which arise at the next order in the derivative expansion. Denoting by Λ the mass scale of the new physics resonances, such interactions are generically suppressed by p/Λ with respect to the ones we consider here, with p characterizing the momenta of the process. Due to the chirality flip, they are further suppressed by y_t/g_*, with g_* a generic BSM coupling satisfying $g_* \leqslant 4\pi$. A notable class of chirality-flipping interactions are dipole-type operators, whose schematic structure is, for example, $\sim \bar{t}_L \sigma^{\mu\nu} t_R Z_\mu p_\nu$. In addition to the previous considerations, dipole operators are not generated at tree level if the transverse SM gauge fields are external to the BSM sector and coupled to it through weak gauging of the corresponding symmetries, as we assume.[1] We also set the triple gauge interactions to their SM values. We choose to do so because in theories where the SM gauge bosons are weakly coupled to the BSM sector, generic deformations of the triple gauge interactions yield small effects in the processes we are interested in [20].[2] Finally, we will also be neglecting the small effects due to the bottom Yukawa coupling.

Theories where the typical scale of the BSM sector can be decoupled from the electroweak scale, $\Lambda/g_* \gg v$, admit a further expansion in the Higgs doublet field H. In such a case BSM effects from heavy resonances can be parameterized by operators of dimension larger than four built out of the SM fields. We are particularly interested in the dim-6 operators [9, 13]

$$\begin{aligned}
\Delta\mathcal{L}_t = {} & \frac{i\bar{c}_L^{(1)}}{v^2} H^\dagger \overleftrightarrow{D_\mu} H \bar{q}_L \gamma^\mu q_L + \frac{i\bar{c}_L^{(3)}}{v^2} H^\dagger \sigma^a \overleftrightarrow{D_\mu} H \bar{q}_L \gamma^\mu \sigma^a q_L \\
& + \frac{i\bar{c}_R}{v^2} H^\dagger \overleftrightarrow{D_\mu} H \bar{t}_R \gamma^\mu t_R + \frac{i\bar{c}_R^b}{v^2} H^\dagger \overleftrightarrow{D_\mu} H \bar{b}_R \gamma^\mu b_R + \left(\frac{i\bar{c}_R^{tb}}{v^2} \tilde{H}^\dagger \overleftrightarrow{D_\mu} H \bar{t}_R \gamma^\mu b_R + \text{h.c.} \right) \\
& + \frac{\bar{c}_u y_t}{v^2} H^\dagger H \bar{q}_L \tilde{H} t_R + \text{h.c.} \,,
\end{aligned} \tag{2.5}$$

[1] Besides, constraints on top dipole moments, either direct from top decay and single top production measurements [24], or indirect from the experimental limits on $b \to s$ transitions [25], are already significant.

[2] Additionally, current bounds on these couplings are already below 10%, and improved sensitivities from diboson production measurements are expected at the 13 TeV LHC run [26].

JHEP01(2016)071

where $\tilde{H} = i\sigma_2 H^*$ and we defined $H^\dagger \overleftrightarrow{D_\mu} H \equiv H^\dagger (D_\mu H) - (D_\mu H)^\dagger H$, etc.. These operators modify the couplings of the top (and bottom) to the W, Z, and h with respect to the SM, such that

$$c_L - 1 = c_L^h = \frac{\bar{c}_L^{(3)} - \bar{c}_L^{(1)}}{1 - \frac{4}{3}s_w^2}\,, \qquad c_{L^b} - 1 = c_{L^b}^h = \frac{\bar{c}_L^{(1)} + \bar{c}_L^{(3)}}{1 - \frac{2}{3}s_w^2}\,, \qquad c_{LL} - 1 = c_{LL}^h = \bar{c}_L^{(3)}\,, \tag{2.6}$$

$$c_R - 1 = c_R^h = \frac{\bar{c}_R}{\frac{4}{3}s_w^2}\,, \qquad c_{R^b} - 1 = c_{R^b}^h = -\frac{\bar{c}_R^b}{\frac{2}{3}s_w^2}\,, \qquad c_{RR} = c_{RR}^h = \bar{c}_R^{tb}\,, \tag{2.7}$$

$$c_t - 1 = \frac{4}{3}c_t^h = -\bar{c}_u\,. \tag{2.8}$$

Notice that at the dim-6 level none of the c_i^h coefficients is independent from the c_i's. Furthermore, while each of the R-handed couplings in eq. (2.7) is affected by an independent dim-6 operator, the deviations in the L-handed ones, eq. (2.6), are partially correlated. This is due to a remnant custodial symmetry of the dim-6 Lagrangian, which is broken by dim-8 operators [27], or absent altogether in the electroweak chiral Lagrangian, see appendix A. The dim-6 operators giving rise to non-standard contributions to the terms in eq. (2.3) can be written as

$$\Delta\mathcal{L}_h = \frac{\bar{c}_H}{2v^2}(\partial_\mu |H|^2)^2 - \frac{\bar{c}_6 \lambda}{v^2}|H|^6\,, \tag{2.9}$$

with $c_V - 1 = -\bar{c}_H/2$ and $c_3 - 1 = \bar{c}_6 - 3\bar{c}_H/2$. The operator $\bar{c}_H$ also contributes to c_t by an amount $-\bar{c}_H/2$. The set of dim-6 operators in eqs. (2.5) and (2.9) encode the leading non-standard effects in theories where both the Higgs and either the L- or R-handed top are strongly coupled to a BSM sector whose generic coupling strength is $g_* > g_{\rm SM}$, with $g_{\rm SM}$ the weak gauge or top Yukawa couplings. In such scenarios the corresponding $\bar{c}$ coefficients can be as large as

$$\bar{c} \lesssim \frac{g_*^2 v^2}{\Lambda^2} \equiv \xi \tag{2.10}$$

with $g_* \leqslant 4\pi$, barring $O(1)$ factors. Particularly relevant examples of such a situation are composite Higgs models with top partial compositeness [10, 11].[3] In such models the need to reproduce the large top Yukawa coupling forces one or both of the top chiral states to couple strongly to the composite sector. We would also like to stress that when $g_* \gg g_{\rm SM}$, the relative importance of probing non-standard top couplings versus direct searches for BSM resonances increases, given that larger values of the resonance mass Λ can be considered.[4]

Out of the BSM effects introduced above, in this work we will mostly focus on the couplings of the top to the Z, c_L and c_R, not only because of their impact on top scattering processes, but also because they are very weakly constrained by direct measurements. Up

[3] In those models the Higgs field arises as a Nambu-Goldstone boson, and the parameter ξ defined in eq. (2.10) is identified with v^2/f^2, where f is the Higgs decay constant.

[4] This is of special relevance, for instance, in composite Twin Higgs models, where the composite resonances, despite being heavy, remain strongly coupled to the Higgs and the top [28–30].

JHEP01(2016)071

to date, the only bound comes from the analysis of $t\bar{t}Z$ production at the 7 TeV LHC [6], from which $O(1)$ deviations in c_L or c_R cannot be excluded. In contrast, other BSM effects are already subject to significant constraints. The most stringent one is on the Zbb coupling: LEP1 measurements directly constrain c_{L^b} at the per-mille level, while the bound on c_{R^b} is at a few per-cent [31]. Due to the former constraint, BSM sectors are typically assumed to couple to q_L such that a custodial P_{LR} symmetry is preserved [32], yielding $c_{L^b} = 1$ to leading approximation. In terms of dim-6 operators, this implies $\bar{c}_L^{(1)} = -\bar{c}_L^{(3)}$. On the other hand, direct bounds on the Wtb coupling coefficients c_{LL} and c_{RR} from single top production [33] and W helicity fraction measurements are around 10% [24, 34]. Notice that in terms of dim-6 operators, the combined constraints on the Zb_Lb_L and Wt_Lb_L couplings, which bound both $\bar{c}_L^{(1)}$ and $\bar{c}_L^{(3)}$, imply BSM effects of at most $\sim 10\%$ on the Zt_Lt_L coupling. However, it should be kept in mind that the experimental status is not yet such as to fully motivate the hypothesis of a large new physics scale Λ compared to the electroweak scale, at least for what regards direct probes of the top sector.

We now turn to the discussion of the indirect bounds. The L- and R-handed top couplings to the W and Z are indirectly probed by electroweak precision data, via top loop contributions to the $\widehat{S}$ and $\widehat{T}$ parameters as well as to the Zb_Lb_L coupling, all of which have been measured with per-mille accuracy. The contribution of $\bar{c}_L^{(1)}$, $\bar{c}_L^{(3)}$, $\bar{c}_R$ to the renormalization group running of the dim-6 operators associated to the aforementioned observables can be consistently computed within the effective theory [13, 20]. For instance, assuming $\bar{c}_L^{(3)} = -\bar{c}_L^{(1)}$ at the scale Λ, the $\widehat{T}$-parameter is renormalized by $\Delta\widehat{T} = N_c y_t^2 (\bar{c}_L^{(1)} - \bar{c}_R) \log(\Lambda/\mu)/(4\pi^2)$, and similar log-divergent terms are generated for $\widehat{S}$ and Zb_Lb_L. Taken at face value, this set of contributions imply the bounds $\bar{c}_L^{(1)}, \bar{c}_R \lesssim 5\%$ [35]. This is analogous to the indirect bound set on $\bar{c}_H$ from log-divergent Higgs loop contributions to $\widehat{S}$ and $\widehat{T}$ [36], which nevertheless does not undermine the relevance of a direct measurement of the hVV ($V = W, Z$) coupling at the LHC. The same logic should apply to direct measurements of the top-Z couplings, even more so after taking into account that, in the cases of interest in this work, $\widehat{S}$, $\widehat{T}$ and Zb_Lb_L are dominated by incalculable ultraviolet (UV) contributions: since it is not protected by any symmetry, $\widehat{S}$ generically receives UV contributions at tree level. On the other hand, even though $\widehat{T}$ and Zb_Lb_L can be UV protected if the BSM sector is custodial and P_{LR} symmetric, contributions to $\widehat{T}$ from top loops with two insertions of $\bar{c}_L^{(1)}$ or $\bar{c}_R$ are actually quadratically divergent and dominant whenever these coefficients are large. The situation is similar for loop contributions to Zb_Lb_L from one insertion of $\bar{c}_L^{(1)} = -\bar{c}_L^{(3)}$ and another of four-fermion operators [13].[5] Finally, we briefly mention bounds from flavor observables. The $\bar{c}_R^{tb}$ coefficient contributes at one loop to the $b \to s\gamma$ decay rate, with an amplitude enhanced by m_t/m_b, and is thus constrained at the per-mille level. In addition, Z-mediated penguin contributions to rare B and K meson decays lead to constraints on $\bar{c}_L^{(1)}$, $\bar{c}_L^{(3)}$ and $\bar{c}_R$ [37], which are at the same level of those from electroweak precision data. All these bounds, however, strongly depend on the assumed underlying flavor structure. In conclusion, currently little can be said with confidence about the couplings of the top to the Z, which motivates the new approach for probing them presented in this work.

[5] The four-fermion operators are irrelevant for the scattering processes we study in this work, but nevertheless large in the same type of BSM scenarios.

JHEP01(2016)071

As far as the couplings of the Higgs boson are concerned, constraints are still relatively mild. Global fits to inclusive signal strengths give $c_V \lesssim 20\%$ [38], whereas searches for the $t\bar{t}h$ signal still allow $O(1)$ deviations in c_t [39–42]. On the other hand, no experimental constraint currently exists on the Higgs cubic coupling c_3, nor on the c_i^h defined in eqs. (2.1), (2.2).

The strength of the constraints discussed above relies on the relative precision of the experimental measurements compared to the BSM effects, which are of size ξ or smaller, see eq. (2.10). In particular, the large uncertainty that affects the LHC measurement of the $t\bar{t}Z$ production cross section is behind the weakness of the direct bounds on modified top-Z couplings. However, there is another avenue for constraining non-standard top interactions, which relies on the large center of mass energies that can be reached at the LHC: departures from the SM prediction of certain top couplings imply that some scattering amplitudes will diverge with the momenta of the process. An analogy can be drawn with $VV \to VV$ scattering, where non-SM values of c_V lead to a growth of the amplitude with energy. In our case, the scatterings of interest are $tV \to tV$ and its crossings. Both in VV and tV scattering, the amplitudes that grow the most with energy involve the longitudinal polarizations of the $W^\pm$ and the Z. For tV scattering this can be clearly seen by inspecting the interactions of the top in a gauge where the Nambu-Goldstone bosons eaten by the W and Z, which we label χ_a ($a = 1, 2, 3$), appear explicitly in the Lagrangian, see eqs. (A.2) and (A.5) in appendix A. For non-SM values of c_L, c_R, etc., four-point contact interactions of the form $\epsilon_{abc}\chi_b\partial_\mu\chi_c(\bar{\psi}\gamma^\mu\psi)_a/v^2$, with $\psi = \{t, b\}$, are generated, implying a p^2/v^2 growth of the amplitudes $\psi\chi \to \psi\chi$. Notice that the symmetry structure of the interaction is such as to include, for example, $tW^\pm \to tW^\pm$, but not $tZ \to tZ$. Likewise, certain scattering amplitudes involving the Higgs, such as $bW^+ \to th$, also display the same divergent behavior at high energies. This follows from the interactions $h\partial_\mu\chi_a(\bar{\psi}\gamma^\mu\psi)_a/v^2$, also shown in appendix A. The relation between the tV and th scattering amplitudes is also obvious when interpreted in terms of dim-6 operators, given the relations in eqs. (2.6)–(2.8). The p^2/v^2 growth should be contrasted with the $m_t p/v^2$ growth that arises if the Higgs couplings c_t or c_V deviate from the SM [15] (see also [43]), whereas no enhancement with energy is generated by deviations in the Higgs cubic coupling c_3. Thus, Higgs coupling modifications only give subleading effects in the high-energy scattering processes we are interested in.

To summarize, in certain two to two scattering processes the sensitivity to non-standard top-Z couplings is enhanced at high energies, possibly overcoming the limited experimental precision. The enhancement scales as $\bar{c}\,p^2/v^2 \sim g_*^2 p^2/\Lambda^2$, which can be much larger than one in models where $g_* \gg 1$, without being in conflict with the effective field theory expansion, that is $p^2 < \Lambda^2$. This approach then takes advantage of the high scattering energies accessible at the LHC. We explicitly demonstrate its effectiveness in the next section, focusing on $tW \to tW$.

3 $tW \to tW$ scattering as case study

Our goal is to study the scattering amplitudes involving tops (and/or bottoms) and W, Z or h that increase at high energies, and to exploit this growth to probe top-Z interactions.

JHEP01(2016)071

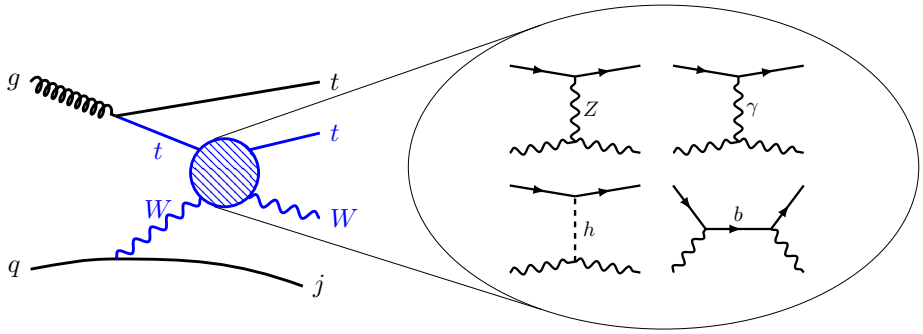

Figure 1. $tW \to tW$ scattering at the LHC. For definiteness, in the inset we show the diagrams corresponding to $tW^- \to tW^-$.

After examining all the possible combinations, we focus on the process $tW \to tW$. Our motivation for this choice is threefold:

1. The amplitude for $tW \to tW$ scattering grows with the square of the energy if either the Zt_Lt_L or the Zt_Rt_R couplings deviate from their SM values.

2. The corresponding collider process, $pp \to t\bar{t}Wj$, gives rise to same-sign leptons (SSL), an extremely rare final state in the SM. This process arises at $O(g_s g_w^3)$ in the gauge couplings, where g_s denotes the strong coupling and g_w any electroweak coupling, as shown in figure 1.

3. The main irreducible background, $pp \to t\bar{t}W + \text{jets}$ at $O(g_s^{2+n} g_w)$ with $n \geq 0$ the number of jets, is insensitive to the details of the top sector, because the W is radiated off a light quark.

The amplitude for two to two scattering processes of the type $\psi_1 + \phi_1 \to \psi_2 + \phi_2$, where $\psi_{1,2} = \{t, b\}$ and $\phi_{1,2} = \{\chi^\pm \equiv (\chi_1 \mp i\chi_2)/\sqrt{2},\ \chi_3, h\}$ are the longitudinal $W^\pm, Z$ or h, is most conveniently expressed in the basis of chirality eigenstate spinors. Retaining only terms that grow with energy, we find

$$\begin{pmatrix} \mathcal{M}_{LL} & \mathcal{M}_{RL} \\ \mathcal{M}_{LR} & \mathcal{M}_{RR} \end{pmatrix} = \frac{\kappa\, g^2}{2m_W^2} \begin{pmatrix} e^{i\varphi}\sqrt{\hat{s}(\hat{s}+\hat{t})}A_{LL} & m_t\sqrt{-\hat{t}}\,A_{RL} \\ -e^{i\varphi}m_t\sqrt{-\hat{t}}\,A_{LR} & \sqrt{\hat{s}(\hat{s}+\hat{t})}A_{RR} \end{pmatrix}, \tag{3.1}$$

where κ and A_{ij} $(i, j = L, R$, with i indicating the chirality of ψ_1 and j the chirality of $\psi_2)$ are process-dependent coefficients.[6] In particular, the A_{ij} encode the dependence on the anomalous couplings: A_{LL} and A_{RR} control the leading amplitudes, which grow as $\hat{s}$, whereas A_{LR} and A_{RL} control the subleading pieces, growing as $\sqrt{\hat{s}}$. All the A_{ij} vanish in the SM, where the amplitude must tend to a constant limit at large $\sqrt{\hat{s}}$. For $tW^- \to tW^-$

[6] We take initial state momenta as ingoing, and final state momenta as outgoing. The Mandelstam variables are defined as $\hat{s} = (p_{\psi_1} + p_{\phi_1})^2$ and $\hat{t} = (p_{\phi_1} - p_{\phi_2})^2$, and φ is the azimuthal angle around the z axis, defined by the direction of motion of ϕ_1.

JHEP01(2016)071

scattering we have $\kappa = 1$ and

$$\begin{aligned} A_{LL} &= -c_{LL}^2 + c_L - \frac{4}{3}s_w^2(c_L - 1)\,, \\ A_{RR} &= -c_{RR}^2 - \frac{4}{3}s_w^2(c_R - 1)\,, \\ A_{LR} &= A_{RL} = \frac{1}{2}\left[(c_L - c_t c_V) - \frac{4}{3}s_w^2(c_L + c_R - 2)\right]. \end{aligned} \tag{3.2}$$

For $tW^+ \to tW^+$, we find again that $\kappa = 1$, A_{LL} and A_{RR} are identical to those in eq. (3.2), whereas the subleading pieces read

$$A_{LR} = A_{RL} = c_{LL}^2 + c_{RR}^2 - \frac{1}{2}\left[(c_L + c_t c_V) - \frac{4}{3}s_w^2(c_L + c_R - 2)\right]. \tag{3.3}$$

We see that whenever $c_L(c_R) \neq 0$ (and barring accidental cancellations), the $LL(RR)$ amplitude grows like $\hat{s}$. This has to be contrasted with the weaker growth like $\sqrt{\hat{s}}$ caused by deviations in the Higgs couplings c_V or c_t. Because their effect is subleading, in our analysis of tW scattering we will set $c_V = c_t = 1$, and focus exclusively on modifications of top-Z interactions. For the latter we will consider two different theoretical interpretations. The first one targets the Zt_Lt_L and Zt_Rt_R couplings, by taking $\Delta_{L,R} \equiv c_{L,R} - 1 \neq 0$ in eq. (2.8), whereas all other coefficients are set to their SM values. Under this assumption, the leading terms in the amplitude read

$$A_{LL} = \left(1 - \frac{4}{3}s_w^2\right)\Delta_L\,, \qquad A_{RR} = -\frac{4}{3}s_w^2\Delta_R\,. \tag{3.4}$$

We note that the sensitivity to Δ_R is lower than to Δ_L due to the s_w^2 suppression of A_{RR}. In addition, we present results in the framework of higher-dimensional operators (HDO), where the deviations in the top-Z couplings are correlated with those in other interactions of the third generation fermions. As discussed in section 2, the per-mille constraint on the Zb_Lb_L vertex forces us to assume $\bar{c}_L^{(3)} = -\bar{c}_L^{(1)}$. We thus take $\bar{c}_L \equiv \bar{c}_L^{(1)} = -\bar{c}_L^{(3)}$ and $\bar{c}_R$ as BSM parameters, whereas all the other $\bar{c}_i$ coefficients in eqs. (2.5) and (2.9) are set to zero. Notice that under these assumptions, $\bar{c}_L$ also modifies the Wt_Lb_L vertex, which contributes to $tW \to tW$ scattering via the b-exchange diagram in figure 1. The leading amplitudes read

$$A_{LL} = -\bar{c}_L^2\,, \qquad A_{RR} = -\bar{c}_R\,. \tag{3.5}$$

We note that in A_{LL} the term linear in $\bar{c}_L$ vanishes. This can be traced back to the absence of the contact interaction $i\chi_+\partial_\mu\chi_-\bar{t}_L\gamma^\mu t_L/v^2 + \text{h.c.}$ when $\bar{c}_L^{(1)} + \bar{c}_L^{(3)} = 0$, see appendix A.

The cross section for $tW \to tW$ scattering is shown in figure 2, assuming representative values of the parameters (Δ_L, Δ_R) and $(\bar{c}_L, \bar{c}_R)$. As we already discussed, while there is a one-to-one correspondence between Δ_R and $\bar{c}_R$, the coupling and HDO hypotheses genuinely differ in the left-handed interactions, because in the HDO case the Wt_Lb_L vertex is also modified. To facilitate the comparison, in figure 2 we choose values of Δ_L and $\bar{c}_L$ that yield the same Zt_Lt_L coupling. The resulting difference is striking: for $\bar{c}_L \neq 0$, the cross section is strongly suppressed compared to the case where $\Delta_L \neq 0$. This is mainly

JHEP01(2016)071

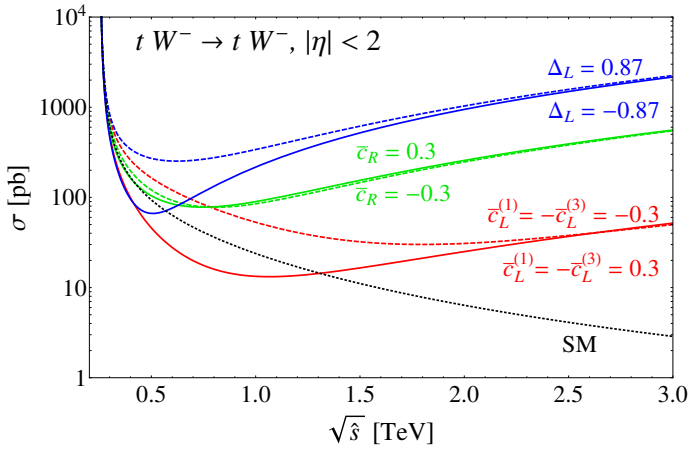

Figure 2. Partonic cross section for the process $tW^- \to tW^-$ as a function of the center of mass energy $\sqrt{\hat{s}}$. The values of Δ_L and $\bar{c}_L^{(1)} = -\bar{c}_L^{(3)}$ are chosen to obtain the same Zt_Lt_L coupling for the blue and red solid curves ($\Delta_L < 0$) and for the blue and red dashed curves ($\Delta_L > 0$). For the Zt_Rt_R coupling there is a one-to-one correspondence between $\bar{c}_R$ and Δ_R, so we show only one set of curves. A pseudorapidity cut $|\eta| < 2$ has been applied to remove the forward singularity, whereas the soft singularity $\hat{s} \to (m_W + m_t)^2$ is evident from the plot. Both singularities arise due to the diagram where a photon is exchanged in the t-channel. At large energy, the red, blue and green curves diverge like $\hat{s}$, whereas the SM cross section (dotted black) falls off as $1/\hat{s}$.

due to the cancellation of the $O(\bar{c}_L)$ piece in the leading amplitude, see eq. (3.5), which implies that the leading term of the cross section is $O(\bar{c}_L^4)$. This in turn translates into a weaker sensitivity to $\bar{c}_L$ with respect to Δ_L, because the latter appears in the leading term of the cross section at $O(\Delta_L^2)$. Additionally, from figure 2 we learn that the cross section is enhanced for all energies, compared to the SM, if $\Delta_L > 0\,(\bar{c}_L < 0)$, while for the opposite sign it is actually suppressed at low values of $\sqrt{\hat{s}}$. Once the LHC parton luminosities are taken into account, we thus expect a weaker sensitivity to the region with $\Delta_L < 0\,(\bar{c}_L > 0)$. The effect is particularly striking for $\bar{c}_L > 0$, in which case the cross section becomes larger than the SM one only well above 1 TeV. These preliminary considerations, which were derived by simple inspection of the cross section of the hard scattering process $tW \to tW$, will find confirmation in the results presented below.

We now turn to the discussion of the $pp \to t\bar{t}Wj$ process at the LHC. In the following we denote our signal, which arises at $O(g_s g_w^3)$, as $(t\bar{t}Wj)_{\rm EW}$, to distinguish it from the leading mechanism for $t\bar{t}W$ production at the LHC, $pp \to t\bar{t}W$+jets at $O(g_s^{2+n} g_w)$ (with $n \geq 0$ the number of jets), which we denote as $(t\bar{t}W{+}{\rm jets})_{\rm QCD}$. Due to its high mass threshold, the latter process was not observed at the Tevatron, therefore the ATLAS and CMS experiments have designed searches aimed at extracting it from 8 TeV LHC data, focusing on the SSL final state and vetoing events that contain a leptonic Z, to remove the contribution from $t\bar{t}Z$ production. The main background is constituted by processes (mostly $t\bar{t}$+jets) giving *misidentified leptons* (misIDℓ), which primarily arise from the decay of heavy flavor hadrons. The latest searches [44, 45] make use of multivariate techniques and thus cannot be straightforwardly reinterpreted, but the CMS cut-and-count analysis [19] contains all the information required to set a first bound on top-Z interactions by exploiting

JHEP01(2016)071

the growth with energy of the $(t\bar{t}Wj)_{\rm EW}$ process. While this search was not optimized for our signal, we will use it to demonstrate the effectiveness of our approach. It is important to notice that since $(t\bar{t}Wj)_{\rm EW}$ is formally of higher order in the weak coupling compared to $(t\bar{t}W{+}{\rm jets})_{\rm QCD}$, it was neglected by CMS in the SSL analysis of ref. [19]. Thus we perform a Monte Carlo (MC) simulation of the signal and apply the cuts chosen by CMS, obtaining the number of events expected in 8 TeV data as function of the parameters (Δ_L, Δ_R) or $(\bar{c}_L, \bar{c}_R)$. We find

$$N_{(t\bar{t}Wj)_{\rm EW}}(\Delta_L,\Delta_R) = 1.6 + 1.0\,\Delta_L + 4.1\,\Delta_L^2 + 0.3\,\Delta_R + 1.1\,\Delta_L\Delta_R + 1.0\,\Delta_R^2\,, \tag{3.6}$$

$$\begin{aligned} N_{(t\bar{t}Wj)_{\rm EW}}(\bar{c}_L,\bar{c}_R) = 1.6 &- 6.2\,\bar{c}_L + 8.7\,\bar{c}_L^2 - 7.0\,\bar{c}_L^3 + 11.2\,\bar{c}_L^4 + 0.8\,\bar{c}_R \\ &- 2.1\,\bar{c}_L\bar{c}_R - 4.1\,\bar{c}_L^2\bar{c}_R + 10.3\,\bar{c}_R^2\,. \end{aligned} \tag{3.7}$$

Notice that the cross section is a polynomial of second order in the coupling deviations $\Delta_{L,R}$, whereas in the HDO case it is of quartic order, because two $\bar{c}_L$ insertions are possible in the diagram with b-exchange, see figure 1. Inspecting eq. (3.6) (eq. (3.7)), we confirm that the pure new physics contributions, which according to the expressions of the leading amplitudes in eq. (3.4) (eq. (3.5)) are proportional to Δ_L^2, Δ_R^2 $(\bar{c}_L^4, \bar{c}_R^2)$, dominate over the interference and the SM terms. In addition, based on the form of the leading amplitudes we expect the following relations to hold approximately: the ratio of the coefficients of Δ_L^2 $(\bar{c}_L^4)$ to Δ_R^2 $(\bar{c}_R^2)$ should be equal to $\left[1 - 3/(4s_w^2)\right]^2 (1)$. These equalities are indeed satisfied within 15%.

For comparison, CMS quotes an expected yield of 14.5 events for $(t\bar{t}W + {\rm jets})_{\rm QCD}$. Thus from eqs. (3.6), (3.7) we see that while in the SM $(t\bar{t}Wj)_{\rm EW}$ only provides a $\sim 10\%$ correction to the $(t\bar{t}W + {\rm jets})_{\rm QCD}$ yield, it grows rapidly moving away from the SM point. This, together with the fact that CMS did not observe any excess over the SM expectation, allows us to set a bound on $\Delta_{L,R}$ or $\bar{c}_{L,R}$. The results are shown in figure 3, where for comparison we also display the bounds obtained from the $t\bar{t}Z$ CMS analysis in the trilepton final state [19], which according to common wisdom provides the best constraint on top-Z couplings at the LHC. Strikingly, we find that the best current constraints are instead provided by the $t\bar{t}W$ channel, so far thought to be insensitive to top-Z interactions. This result becomes even more remarkable when we consider that the CMS analysis was optimized to increase the sensitivity not to our signal, but to the main irreducible background $(t\bar{t}W{+}{\rm jets})_{\rm QCD}$. Inspecting the HDO bound in the right panel of figure 3, we note that the coefficients of the dim-6 operators are allowed to be of $O(1)$. Thus the interpretation of the result in terms of HDO is not truly justified, and should be intended as purely illustrative of the current sensitivity. Assuming only a modification of the Zt_Rt_R coupling, we find for 8 TeV, 19.5 fb^{-1} at 95% CL[7]

$$-3.6 < \Delta_R < 2.4 \qquad \text{or} \qquad -1.13 < \bar{c}_R < 0.74\,. \tag{3.8}$$

[7]Given the very large Ztt coupling deviations allowed by 8 TeV data, one may wonder about effects in the $t\bar{t}$ forward-backward asymmetry measured at the Tevatron. The tree-level contribution due to $q\bar{q} \to Z, \gamma \to t\bar{t}$ is $\sim 0.2\%$ in the SM [46], and we estimate that, within the allowed region shown in the left panel of figure 3, it is enhanced by a factor $\lesssim 5$, thus remaining strongly subdominant to the QCD contribution, which amounts to approximately 8% [46]. Interestingly, at the LHC the $t\bar{t}$ charge asymmetry in the $t\bar{t}W$ process is significantly larger than in inclusive $t\bar{t}$ production [47].

JHEP01(2016)071

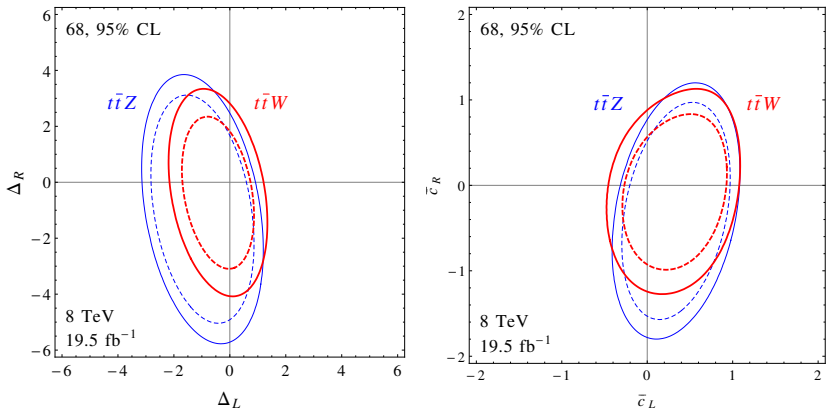

Figure 3. In red, the constraints on top-Z coupling deviations (left panel) and HDO coefficients (right panel) derived from the $t\bar{t}W$ analysis at 8 TeV. For comparison, in blue we show the constraint obtained from the 8 TeV $t\bar{t}Z$ analysis.

Having proven the effectiveness of our method, we move on to designing a search at 13 TeV that specifically targets the process $(t\bar{t}Wj)_{\rm EW}$. The latter has two distinctive features that can be exploited to separate it from the background: a tW pair with large invariant mass (where t can be either top or antitop, and W either of $W^\pm$), due to the growth with energy of the hard scattering process, and a highly energetic forward jet arising from the radiation of a W off an initial-state quark. We devise cuts that single out events with these properties and thus increase the significance of the signal over the background, which is mainly composed by $(t\bar{t}W{+}{\rm jets})_{\rm QCD}$ and misIDℓ. We validate our background simulations against the CMS 8 TeV results, and perform the cut optimization using the point $(\Delta_L, \Delta_R) = (0, 1)$ as signal benchmark. This choice is motivated by the fact that the Zt_Rt_R coupling is currently very weakly constrained even under the assumption of heavy new physics, in contrast with the Zt_Lt_L coupling, which within the HDO framework is already bounded by the measurements of Zb_Lb_L and of Wt_Lb_L. Our basic selection requires two SSL and ≥ 4 jets, among which ≥ 1 must be b-tagged. We identify a set of useful kinematic variables to enhance the significance of the signal, which are discussed in detail in section 4.3.1. For illustration, in figure 4 we show the normalized distributions of signal and backgrounds for a subset of these variables: the transverse momentum of the leading lepton, $p_T^{\ell_1}$, the invariant mass of the two leading leptons, $m_{\ell_1\ell_2}$, and the pseudorapidity of the forward jet, $|\eta_{j_{\rm fw}}|$. It is apparent that the leptonic variables are effective in suppressing the misIDℓ background, whereas a lower cut on the pseudorapidity of the forward jet helps to suppress $(t\bar{t}W{+}{\rm jets})_{\rm QCD}$. The event yields after all cuts, assuming an integrated luminosity of 300 fb^{-1}, are given by

$$N_{(t\bar{t}Wj)_{\rm EW}}(\Delta_L, \Delta_R) = 16.9 + 12.7\,\Delta_L + 172.4\,\Delta_L^2 + 0.5\,\Delta_R + 37.2\,\Delta_L\Delta_R + 40.8\,\Delta_R^2\,, \tag{3.9}$$

$$\begin{aligned} N_{(t\bar{t}Wj)_{\rm EW}}(\bar{c}_L, \bar{c}_R) = 16.7 &- 73.2\,\bar{c}_L + 145.0\,\bar{c}_L^2 - 164.2\,\bar{c}_L^3 + 408.3\,\bar{c}_L^4 + 6.3\,\bar{c}_R \\ &- 4.1\,\bar{c}_L\bar{c}_R - 121.8\,\bar{c}_L^2\bar{c}_R + 412.3\,\bar{c}_R^2\,. \end{aligned} \tag{3.10}$$

JHEP01(2016)071

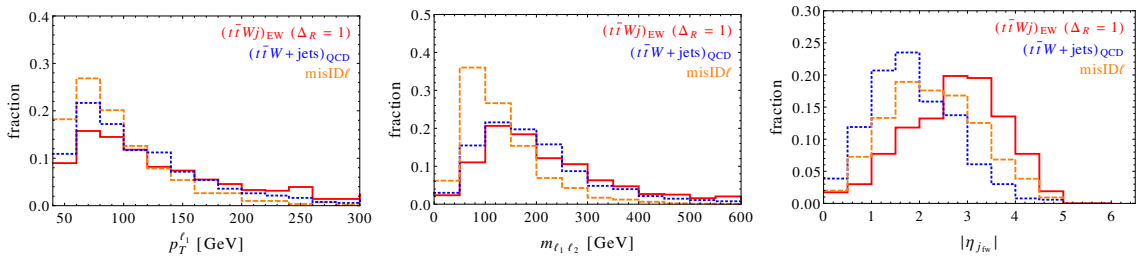

Figure 4. Normalized distributions for the signal $(t\bar{t}Wj)_{\rm EW}$ and the two main backgrounds $(t\bar{t}W+{\rm jets})_{\rm QCD}$ and misIDℓ at 13 TeV, after the $4j$ pre-selection.

The expected background yield is of 51 events for $(t\bar{t}W+{\rm jets})_{\rm QCD}$, and of 34 events for misIDℓ. By performing a simple likelihood analysis, we obtain the constraints on $\Delta_{L,R}$ and $\bar{c}_{L,R}$ shown as red contours in figure 5. The solid contours assume no systematic uncertainty on the background, whereas the dotted contours include the dominant 50% systematic uncertainty on the misIDℓ component. For comparison, in the same figure we show the projected 13 TeV bounds from the $t\bar{t}Z$ process, as derived in ref. [6]. This comparison is meant to be illustrative, because the projection of ref. [6] is based on a NLO-QCD analysis of the signal, without the inclusion of detector effects nor backgrounds. The two main effects that were gleaned by inspecting the partonic cross section in figure 2 are now manifest in figure 5. First, the sensitivity to $\bar{c}_L$ is weaker than to Δ_L, because the former appears in the leading term of the cross section at $O(\bar{c}_L^4)$ while the latter at $O(\Delta_L^2)$, see eqs. (3.4) and (3.5). Second, the $\bar{c}_L > 0$ direction is less strongly constrained than $\bar{c}_L < 0$, because in the former case the partonic cross section for $tW \to tW$ scattering is smaller than the SM one for $\sqrt{\hat{s}} \lesssim$ TeV, where the bulk of the LHC parton luminosity is concentrated. Comparing with the $t\bar{t}Z$ process, we find that our $t\bar{t}W$ analysis gives a significantly stronger bound on the coupling deviations $\Delta_{L,R}$, and comparable sensitivity to the HDO coefficients $\bar{c}_{L,R}$. We also note that in the HDO case the shape of the $t\bar{t}W$ contours is rather different from that of the $t\bar{t}Z$ ones, leading to an interesting complementarity of the two measurements. Assuming only a modification of the Zt_Rt_R coupling, our analysis gives for 13 TeV, 300 fb^{-1} at 95% CL

$$-0.83 < \Delta_R < 0.74 \qquad \text{or} \qquad -0.26 < \bar{c}_R < 0.23\,, \tag{3.11}$$

with no systematics on the background, while if a 50% systematic uncertainty on the misIDℓ component is included, we find $-1.04 < \Delta_R < 0.95$ or $-0.32 < \bar{c}_R < 0.30$. Based on these results, we urge the ATLAS and CMS collaborations to search for the $(t\bar{t}Wj)_{\rm EW}$ signal in the upcoming 13 TeV data. The necessary technical details of our analysis are presented in the next section, which the reader interested only in the discussion of our results can omit, to move directly to section 5.

4 $t\bar{t}W$ analysis

In this section we present the technicals details of our analysis. Frequent reference will be made to the 8 TeV CMS cut-and-count search for $t\bar{t}W$ [19], based on the requirements of

JHEP01(2016)071

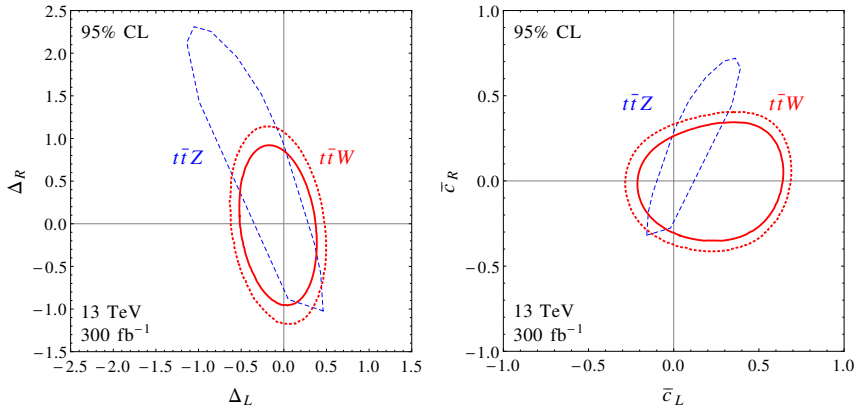

Figure 5. In red, the constraints on top-Z coupling deviations (left panel) and HDO coefficients (right panel) derived from our $4j$ $t\bar{t}W$ analysis at 13 TeV. The solid contour assumes no systematic uncertainty on the background, whereas the dotted one includes a 50% systematic on the misIDℓ component. For comparison, in dashed blue we show the constraint obtained from $t\bar{t}Z$, as derived in ref. [6] by means of a NLO-QCD signal-only analysis.

two SSL and a leptonic Z veto. After reinterpreting this search to obtain the 8 TeV bounds on top-Z interactions, we employ its results to validate our background simulations. We then propose a dedicated 13 TeV analysis that targets the signal process $(t\bar{t}Wj)_{\rm EW}$.

4.1 8 TeV bounds

The SSL analysis of ref. [19] was aimed at measuring the $(t\bar{t}W{+}\text{jets})_{\rm QCD}$ process, while our signal process $(t\bar{t}Wj)_{\rm EW}$ was neglected. On the other hand, the $(t\bar{t}Wj)_{\rm EW}$ amplitude interferes with the one-jet component of $(t\bar{t}W{+}\text{jets})_{\rm QCD}$, which we will label $(t\bar{t}Wj)_{\rm QCD}$, thus *a priori* our signal cannot be generated separately from the $(t\bar{t}W{+}\text{jets})_{\rm QCD}$ process. A further subtlety arises because the $t\bar{t}W$ final state can also be produced purely from weak interactions, at $O(g_w^3)$. To quantify these effects, we compute inclusive parton-level cross sections for the SM and one representative signal point, which is chosen to be $\Delta_R = 3.2$ at 8 TeV and $\Delta_R = 1$ at 13 TeV, roughly corresponding to the sensitivity of our analysis (see figures 3 and 5, respectively). The cross sections are computed with MadGraph5 [49], employing a FeynRules [50] model that allows us to add to the SM either the corrections $\Delta_{L,R}$ to the top-Z couplings, or the dim-6 operators proportional to $\bar{c}_L^{(1)}, \bar{c}_L^{(3)}, \bar{c}_R$. The model was validated against analytical computations of several $2 \to 2$ amplitudes, and employed for all the MC simulations used in this paper. For the SM parameters we take the values

$$\begin{aligned} m_Z &= 91.19\ \text{GeV}\,, \qquad \alpha(m_Z) = 1/127.9\,, \qquad G_F = 1.166 \times 10^{-5}\ \text{GeV}^{-2}\,, \\ \alpha_s(m_Z) &= 0.1184\,, \qquad\qquad m_t = 173\ \text{GeV}\,. \end{aligned} \tag{4.1}$$

Inspection of the inclusive cross sections in table 1 shows that the pure electroweak contribution to $t\bar{t}W$ is very small, thus we will neglect it in our study. On the other hand, the effect of the interference between the $(t\bar{t}Wj)_{\rm QCD}$ and $(t\bar{t}Wj)_{\rm EW}$ amplitudes on the deviation from the SM cross section in presence of anomalous top-Z couplings is at most 20%.

JHEP01(2016)071

		$(t\bar{t}W)_{\rm QCD}$	$(t\bar{t}W)_{\rm EW}$	$(t\bar{t}Wj)_{\rm QCD}$	$(t\bar{t}Wj)_{\rm EW}$	$(t\bar{t}Wj)_{\rm full}$	$1-\frac{\delta_{\rm full}}{\delta_{\cancel{\rm int}}}$
8 TeV	SM	130.6	0.99	94.0	12.6	104.1	0.19(4)
	$\Delta_R = 3.2$	130.6	1.73	94.0	64.9	146.5	
13 TeV	SM	347.9	2.85	341.3	56.0	386.1	0.02(15)
	$\Delta_R = 1$	347.9	2.71	341.3	94.6	423.9	

Table 1. Parton-level cross sections in femtobarns. By $(t\bar{t}Wj)_{\rm full}$ we denote the full amplitude including the interference. For the $t\bar{t}Wj$ process we imposed the cuts $p_T^j > 20$ GeV and $|\eta| < 5$. The quantity $\delta_{\rm full,\cancel{int}} \equiv \sigma^{\Delta_R\neq 0}_{(t\bar{t}Wj)_{\rm full,\,EW}} - \sigma^{\rm SM}_{(t\bar{t}Wj)_{\rm full,\,EW}}$ is the deviation from the SM, computed either including ('full') or neglecting ('~~int~~') the interference. In the last column, the uncertainty in parentheses refers to the last digit.

Given the exploratory nature of our study, for simplicity we choose to perform our analysis neglecting the interference, and take into account its effect by including a conservative 20% systematic uncertainty on the $(t\bar{t}Wj)_{\rm EW}$ signal.

Because we neglect the interference, to compute the constraints on top-Z interactions we need to apply the CMS cuts to the $(t\bar{t}Wj)_{\rm EW}$ process, and extract the dependence of the signal event yield on the parameters $\Delta_{L,R}$ and $\bar{c}_{L,R}$. The signal yield will then be summed to those of the processes already simulated in ref. [19], including $(t\bar{t}W + \text{jets})_{\rm QCD}$. Signal events are generated with MadGraph5, employing our FeynRules model. Showering and hadronization effects are accounted for with Pythia 6.4 [51], and the detector simulation is performed using PGS4 [52]. To match ref. [19], the following changes are made to the default CMS settings in PGS: the b-tagging is modified to reproduce the performance of the medium working point of the CSV algorithm, and the jet reconstruction algorithm is set to anti-k_T with distance parameter of 0.5. In addition, the calorimeter coverage for jets is extended up to $|\eta| = 5$. We make use of NN23LO1 parton distribution functions [53], and factorization and renormalization scales are set to the default MadGraph5 event-by-event value. Unless otherwise noted, the above settings are used for all the event samples used in this paper. The event selection requirements follow closely those listed in section 4 of ref. [19], and are as follows:

1. Two SSL, each with $|\eta| < 2.4$ and $p_T > 40$ GeV;

2. At least three jets with $|\eta| < 2.4$ and $p_T > 30$ GeV, among which at least one must be b-tagged;

3. An event is rejected if it contains, in addition to the SSL pair, 2 or more leptons with $|\eta| < 2.4$ and $p_T > 10$ GeV, or if it contains one such lepton forming, with one of the two SSL, a same-flavour opposite-sign pair whose invariant mass is within 15 GeV of m_Z;

4. $H_T > 155$ GeV, where H_T is the scalar sum of the transverse momenta of all jets as defined in point 2;

JHEP01(2016)071

$(t\bar{t}W+\text{jets})_{\text{QCD}}$	misIDℓ	irreducible	$t\bar{t}Z$	misIDQ	WZ	total	observed
14.5	12.1	5.8	3.9	2.2	1.3	39.8	36

Table 2. Expected and observed background yields for the 8 TeV SSL analysis, after summing over all SSL categories. The numbers are taken from ref. [19].

5. The CMS lepton isolation is approximated by requiring that $\Delta R(\ell, j) > 0.3$ for each of the SSL and for all jets as defined in point 2.

The events are divided in 6 categories depending on the flavor/charge combination of the SSL. The expected event yields for all the processes considered in ref. [19], after summing over all SSL categories, are shown in table 2. The largest SM contribution is given by $(t\bar{t}W+\text{jets})_{\text{QCD}}$, which was considered as signal in ref. [19], but will be a background in our analysis. The second contribution is given by the misIDℓ background, composed of processes with one prompt and one non-prompt lepton. The latter arises from the decay of a heavy flavor hadron, and is misidentified as prompt. The misIDℓ background is dominated by $t\bar{t}$ events. Subleading contributions are given by the 'irreducible' processes, which include $t\bar{t}h$ and same-sign WW production in association with jets, and by $t\bar{t}Z$. A minor background is given by processes where the misidentification of the charge of one electron leads to the SSL final state. This contribution, dominated by $t\bar{t}$ and Drell-Yan (DY)+jets events, is labeled *misidentified charge* (misIDQ) background. Finally, WZ+jets production is also a minor background.

To efficiently compute the signal yield after cuts as function of the parameters $\Delta_{L,R}$ and $\bar{c}_{L,R}$, we exploit the fact that formally the $(t\bar{t}Wj)_{\text{EW}}$ cross section is a polynomial of second order in $\Delta_{L,R}$, and of quartic order in $\bar{c}_{L,R}$. Thus it is sufficient to generate a small number of signal samples and perform a fit, which yields semi-numerical formulas parameterizing the signal predictions. For brevity, only the sum over all flavor/charge combinations of the SSL was reported in eqs. (3.6), (3.7). The statistical uncertainty on the signal yields computed using those equations is approximately 10%. The fact that CMS observed a number of events compatible with the SM prediction (see table 2) allows us to set a bound on top-Z interactions. Denoting by $\vec{p}$ either $\{\Delta_L, \Delta_R\}$ or $\{\bar{c}_L, \bar{c}_R\}$, we thus consider the following likelihood

$$
\begin{aligned}
L(\vec{p}; r, t) &= \prod_{i=1}^{6} \frac{(N^i_{S+B})^{N^i_{\text{obs}}} e^{-N^i_{S+B}}}{N^i_{\text{obs}}!} P_{\sigma_r}(r,1) P_{\sigma_t}(t,1)\,, \\
P_\sigma(x, x_0) &= \frac{1}{\frac{1}{2}\left[1 + \text{erf}\left(\frac{1}{\sqrt{2}\,\sigma}\right)\right]} \frac{1}{\sqrt{2\pi}\sigma} e^{-\frac{(x-x_0)^2}{2\sigma^2}}\,, \\
N^i_{S+B} &= r N^i_{B,\,\text{misID}\ell} + N^i_{B,\,\text{other}} + N^i_{(t\bar{t}Wj)_{\text{EW}}}(\vec{0}) + t(N^i_{(t\bar{t}Wj)_{\text{EW}}}(\vec{p}) - N^i_{(t\bar{t}Wj)_{\text{EW}}}(\vec{0}))\,,
\end{aligned}
\tag{4.2}
$$

where the dominant systematic uncertainty of 50% on the misIDℓ background was included[8]

[8] We have verified that by assuming 50% on the misIDℓ background as the only systematic uncertainty, we reproduce to good accuracy the measurement of the $t\bar{t}W$ cross section quoted in ref. [19]: we find 178^{+106}_{-101} fb, to be compared with 170^{+114}_{-106} fb.

JHEP01(2016)071

by setting $\sigma_r = 0.5$, and we also took into account the already mentioned 20% systematic uncertainty on the signal by setting $\sigma_t = 0.2$. The index i runs over the 6 SSL categories. Maximizing the marginalized log-likelihood, defined as $\ell_m(\vec{p}) = \log\left(\int_0^{+\infty} L(\vec{p}; r, t) dr\, dt\right)$, and taking standard confidence intervals we obtain the exclusion contours shown in figure 3. To put our constraints in perspective, we compare them with those derived from the CMS 8 TeV $t\bar{t}Z$ analysis in the trilepton final state, also performed in ref. [19] (see appendix B for details). Setting $\Delta_L = 0$ (or equivalently, $\bar{c}_L = 0$) in the likelihood, we obtain the one-dimensional bounds reported in eq. (3.8). Notice that, as shown in table 2, despite the leptonic Z veto the $t\bar{t}Z$ process gives a small contribution to the SSL signal region. For the sake of consistency, to generate the $t\bar{t}W$ contours in figure 3 we have taken into account the dependence of the $t\bar{t}Z$ event yield on the parameters $\vec{p}$, rescaling the value quoted by CMS for the SM (3.9 events) by the ratio $\sigma_{t\bar{t}Z}(\vec{p})/\sigma^{\rm SM}_{t\bar{t}Z}$, with $\sigma_{t\bar{t}Z}$ the inclusive cross section for $pp \to t\bar{t}Z$ at 8 TeV. This is based on the assumption that the selection efficiency is independent of $\vec{p}$, which is expected to be a reasonable approximation, since the leading $pp \to t\bar{t}Z$ amplitude does not grow with energy for non-SM top-Z couplings. On the other hand, the subleading contribution $pp \to t\bar{t}Zj$, which is the analogue of our signal with $W \to Z$, does grow with energy, and one may wonder if it is justified to discard it. However, as discussed in section 5.4, the $tZ \to tZ$ amplitude only grows with energy as $\sqrt{\hat{s}}$, as opposed to $\hat{s}$ for $tW \to tW$. We can thus safely neglect this piece. The effect of the $t\bar{t}Z$ contamination on the $t\bar{t}W$ bounds in figure 3 is small.

4.2 Background simulation

To set bounds from the 8 TeV CMS data, it was sufficient to simulate the $(t\bar{t}Wj)_{\rm EW}$ signal and make use of the expected background yields quoted by CMS. Thus it was not necessary to simulate all the backgrounds listed in table 2. However, because our aim is also to devise an analysis at 13 TeV, which we will specifically tailor to improve the sensitivity to top-Z interactions, we first need to make sure that our simulation can reproduce the 8 TeV results contained in ref. [19] for all the processes listed in table 2. The salient features of the simulation are summarized below for each background. Unless otherwise specified, jet matching is performed using the shower $k_\perp$ scheme [54] with matching scale set to 30 GeV, and the definition of jet includes b-jets.

- $(t\bar{t}W{+}\text{jets})_{\rm QCD}$: we generate a matched sample of $t\bar{t}W + 0, 1$ jets, and normalize it to the NLO cross section of 206 fb [19]. Notice that in ref. [55] the $(t\bar{t}Wj)_{\rm QCD}$ component was shown to have dramatic effects in some regions of phase space. However, the NLO corrections to $(t\bar{t}Wj)_{\rm QCD}$ were also computed, finding that they have a small effect.[9] This supports the use of a LO matched sample with $0, 1$ jets, at least for our exploratory analysis.

- MisIDℓ: CMS estimated this background by means of a data-driven method. We follow the approach of ref. [48], where it was proposed to exploit the relationship between the misidentified (or 'fake') lepton and the heavy flavor jet from which it

[9] We thank F. Maltoni for pointing this out to us.

JHEP01(2016)071

originated. The method consists of applying certain probability and transfer functions to MC events containing heavy flavor jets. In our case, we consider a matched sample of $t\bar{t}+0,1,2$ jets, normalized to the NNLO cross section of 245.8 pb [56]. More details about the method are given in appendix C. Here we only stress that the overall efficiency of the fake lepton generation is a free parameter of the method, and we simply fix it to reproduce the CMS yield reported in table 2.

- Irreducible: this background is composed mainly by $\bar{t}t$ production in association with a Higgs, with a $\sim 10\%$ component of same-sign WW. For the former process, we generate a matched sample of $t\bar{t}h+0,1$ jets, and normalize it to the NLO cross section of 129.3 fb [57]. For the latter, we generate $W^{\pm}W^{\pm}+3j$ with matching, with LO normalization.

- $t\bar{t}Z$: we generate a matched sample of $t\bar{t}Z+0,1$ jets, and normalize it to the NLO cross section of 197 fb [19].

- misIDQ: this background was estimated by CMS using a combination of data and MC. We mimic their method by selecting MC events that contain opposite-sign $e\mu$ or ee and pass all the cuts except for the same-sign requirement, and weighting them with the probability for the charge of each electron to be mismeasured (the probability of the charge of a μ being mismeasured is negligible). We take the probabilities to be 2.3×10^{-3} for the endcaps ($|\eta|>1.479$) and 2×10^{-4} for the barrel ($|\eta|<1.479$) [58]. These probabilities correspond to the 'selective' charge identification method [58], and agree with the order-of-magnitude values quoted in ref. [19]. Two processes contribute: $t\bar{t}$, and DY+jets. For the former, which amounts to $\sim 70\%$ of the total, we generate a matched sample of $t\bar{t}+0,1,2$ jets, normalized to the NNLO cross section of 245.8 pb [56]. For the latter, we generate a sample of $\ell^+\ell^-+3j$ with matching, with LO normalization.

- WZ: we generate $WZ+3j$ with matching and LO normalization.

For each of the above processes, we compare the distributions of the leading lepton p_T and H_T with those reported in figure 2 of ref. [19]. The shapes of the distributions are reproduced in all cases, including misIDℓ and misIDQ, which were predicted by CMS using data. This gives us, in particular, confidence in our treatment of the fake leptons, which together with $(t\bar{t}W+\text{jets})_{\text{QCD}}$ will dominate the background in the 13 TeV analysis. On the other hand, as shown in table 3, the normalization agrees reasonably well with the CMS result for all the processes except misIDQ, for which our simulation overestimates the event yield by a factor ~ 3.5. Nevertheless, once we normalize to the CMS rate, the misIDQ distributions are reproduced to good accuracy. In addition, we checked that for all processes we reproduce, within errors, the relative contributions to the 6 SSL categories shown in table 1 of ref. [19]. The 8 TeV distributions for $(t\bar{t}W+\text{jets})_{\text{QCD}}$ and misIDℓ are shown in figure 6, after normalization to the respective CMS yields. Having validated our background simulations against data, we will confidently make use of them in the 13 TeV analysis, by generating each process with the same settings employed at 8 TeV, including jet

JHEP01(2016)071

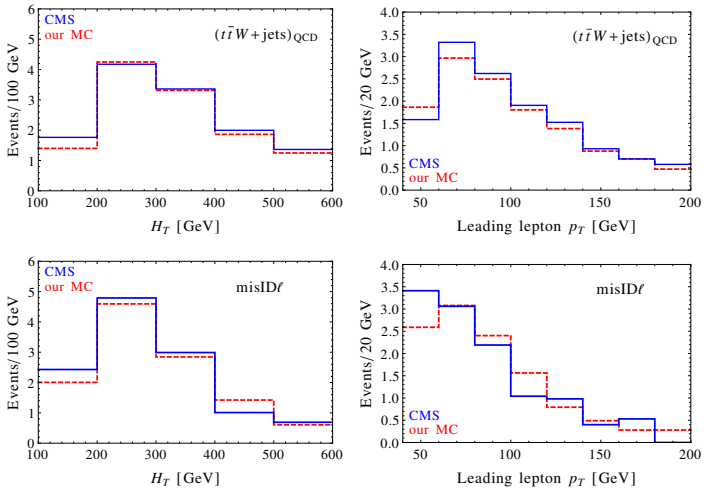

Figure 6. 8 TeV distributions for $(t\bar{t}W+\text{jets})_{\text{QCD}}$ (upper row) and misIDℓ (lower row). The blue histograms show the CMS result, whereas the red histograms show our prediction, after normalizing to the CMS total yields.

	$(t\bar{t}W+\text{jets})_{\text{QCD}}$	misIDℓ	irreducible	$t\bar{t}Z$	misIDQ	WZ
$\frac{\text{CMS}}{\text{our MC}}$	0.62	—	1.09	1.20	0.28	0.83

Table 3. Multiplicative factors we need to apply to the normalization of our MC samples to match the CMS results in table 2. The normalization of the misIDℓ background is not predicted by the fake lepton simulation.

	$(t\bar{t}W+\text{jets})_{\text{QCD}}$	$t\bar{t}$ (misIDℓ, misIDQ)	$t\bar{t}h$	$t\bar{t}Z$
$\sigma_{13\text{ TeV}}$	566.3 fb [59]	788.2 pb [60]	508.5 fb [61]	771 fb [59]

Table 4. Inclusive cross sections used to normalize the 13 TeV samples. The $t\bar{t}$ cross section is at approximate NNLO, whereas the others are at NLO. For the processes not listed here, LO normalization was used.

multiplicity. The normalization will be fixed to the best available calculation (see table 4), multiplied by the rescaling factor given in table 3, which brings our 8 TeV rate in agreement with the one predicted by CMS.[10] The misIDℓ process will be simulated with the same parameters that match the CMS results at 8 TeV, because we do not expect a significant variation going to the higher collider energy.

4.3 13 TeV analysis

The $(t\bar{t}Wj)_{\text{EW}}$ process is characterized by the presence of a highly energetic forward jet, which provides a natural handle to separate the signal from the background. In our analysis, we thus select a candidate forward jet, and make use of kinematic variables constructed

[10]The irreducible and misIDQ backgrounds are composed by two distinct processes. In these cases, the rescaling factor of table 3 is applied to each of the component processes.

JHEP01(2016)071

out of it. However, forward jet tagging is known to face issues in high-pileup conditions, like those of LHC Run-2, and what level of performance will be achieved is still an open question. Interestingly, it was suggested [62], in the context of a study of heavy top partners in the very $t\bar{t}Wj$ final state, that clustering forward jets with a radius parameter smaller than the standard one can greatly improve the forward jet tagging. Yet in our analysis we go beyond tagging, making use of the reconstructed four-momentum of the forward jet. Because this aspect of the analysis may be affected by pileup, we choose to also perform a separate analysis where we do not make any reference to forward jets, and only employ central jets with $|\eta| < 2.4$. The results of this second analysis (which will be labeled $3j$ analysis) are very robust and likely conservative, whereas the first ($4j$ analysis) illustrates the potential of forward jet variables in suppressing the background.

4.3.1 $4j$ analysis

In the $4j$ analysis, we make use of the forward jet that characterizes the signal. The event pre-selection requires the following:

1. The cuts on leptons are identical to the 8 TeV analysis;
2. We require at least four jets with $p_T > 30\,\text{GeV}$ and $|\eta| < 5$, among which at least three must be central, i.e. must satisfy $|\eta| < 2.4$ (at least one of the central jets must be b-tagged), and at least one must not be b-tagged;
3. No cut is applied on H_T, defined as the scalar sum of the p_T of all the central jets as defined in point 2;
4. The CMS lepton isolation is approximated by requiring that $\Delta R(\ell, j) > 0.3$ for each of the SSL and for all central jets.

After the pre-selection, to find the best set of cuts we perform an optimization based on the signal point $(\Delta_L, \Delta_R) = (0, 1)$, which corresponds roughly to the target sensitivity at 13 TeV with $300\,\text{fb}^{-1}$. For the optimization, we include only the two main backgrounds $(t\bar{t}W + \text{jets})_{\text{QCD}}$ and misIDℓ. The optimization is performed by maximizing the statistical significance of the exclusion[11]

$$\mathcal{S} \equiv \frac{S}{\sqrt{S+B}} = \frac{N_{(t\bar{t}Wj)_{\text{EW}}}(\Delta_R = 1) - N_{(t\bar{t}Wj)_{\text{EW}}}(\text{SM})}{\sqrt{N_{(t\bar{t}Wj)_{\text{EW}}}(\Delta_R = 1) + N_{(t\bar{t}W+\text{jets})_{\text{QCD}}} + N_{\text{misID}\ell}}}\,, \tag{4.3}$$

where S and B indicate the signal and background, respectively. The luminosity is assumed to be 300 fb^{-1}. We consider a number of candidate variables in order to enhance $\mathcal{S}$. The best are found to be the transverse momentum of the leading lepton, $p_T^{\ell_1}$, the invariant mass of the two leading leptons, $m_{\ell_1\ell_2}$, the missing transverse energy, MET, the scalar sum of H_T and the p_T of the two leading leptons, S_T, and two angular variables that involve the forward jet, namely $|\eta_{j_{\text{fw}}}|$ and $\Delta\eta \equiv |\eta_{j_{\text{fw2}}} - \eta_{j_{\text{fw}}}|$, where the forward jet j_{fw} and the 'second forward jet' j_{fw2} are defined as

[11] The 95% CL exclusion corresponds to $\mathcal{S} \simeq 1.64$.

JHEP01(2016)071

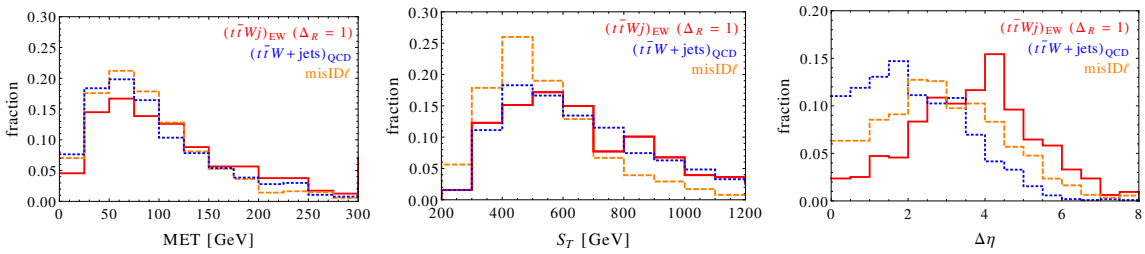

Figure 7. Normalized distributions for $(t\bar{t}Wj)_{\rm EW}$ and the two main backgrounds $(t\bar{t}W{+}{\rm jets})_{\rm QCD}$ and misIDℓ at 13 TeV, after the $4j$ pre-selection. The other relevant distributions were shown in figure 4.

- $j_{\rm fw}$ is the non-b-tagged jet with largest $|\eta|$,
- $j_{\rm fw2}$ is the jet with the largest invariant mass with $j_{\rm fw}$.

The normalized signal and background distributions of these variables after the pre-selection cuts are shown in figures 4 and 7. The cut-flow for our optimal cuts is in table 5. We see that the cuts on the leptons effectively suppress the fake lepton background, while the cuts on the forward jet are successful against the $(t\bar{t}W{+}{\rm jets})_{\rm QCD}$ background. After all cuts, we achieve a significance of 3.5 and a signal to background ratio of approximately 0.4. In table 6 we report the event yields for the subleading backgrounds. We note that because our selection requires at least 4 jets, the backgrounds $W^\pm W^\pm, WZ$ and DY should in principle be simulated with four extra partons in the matrix element, matched to the parton shower. This requires, however, a large computational effort, which goes beyond the scope of this paper. Therefore, as an estimate, we simply simulate these backgrounds with 3 additional partons at matrix element level. We find that all three processes give a very small contribution to the signal region. In particular, DY+jets is very strongly suppressed by the MET cut. The signal yields after all cuts were given in eqs. (3.9), (3.10). The statistical uncertainty on the signal yields computed using those equations is approximately 10%. To derive the constraints on the parameters $\vec{p}$, we perform a single-bin[12] likelihood analysis, in complete analogy with eq. (4.2), assuming the observed number of events to equal the SM prediction. We also consistently take into account the dependence of the subleading background $t\bar{t}Z$ on the parameters $\vec{p}$, by rescaling the yield in table 6 with the ratio $\sigma_{t\bar{t}Z}(\vec{p})/\sigma^{\rm SM}_{t\bar{t}Z}$, with $\sigma_{t\bar{t}Z}$ the inclusive cross section for $pp \to t\bar{t}Z$ at 13 TeV. The resulting bounds were shown as red contours in figure 5. In addition to the 20% systematic uncertainty on the signal, we assume either no systematics on the background (solid contours), or 50% systematic uncertainty on the misIDℓ component (dotted). For comparison, we also show in dashed blue the results of the $t\bar{t}Z$ projection made in ref. [6]. Assuming that the only deformation of the SM is a modification of the Zt_Rt_R coupling, we obtain the one-dimensional bounds reported in eq. (3.11).

[12] We have verified that taking one inclusive bin instead of 6 SSL categories makes the 8 TeV bounds only slightly weaker.

JHEP01(2016)071

	$\mathcal{S}$	EW(SM)	EW($\Delta_R = 1$)	$(t\bar{t}W$+jets$)_{\rm QCD}$	misIDℓ	S/B
pre-selection	2.8	91	183	445	476	0.091
$p_T^{\ell_1} > 100\,\text{GeV}$	3.0	44	111	223	166	0.15
$m_{\ell_1\ell_2} > 125\,\text{GeV}$	3.1	39	102	202	112	0.18
MET $> 50\,\text{GeV}$	3.2	28	84	152	80	0.22
$\lvert\eta_{j_{\rm fw}}\rvert > 1.75$	3.4	21	69	77	58	0.31
$\Delta\eta > 2$	3.5	20	67	60	49	0.36
$S_T > 500\,\text{GeV}$	3.5	16	58	51	34	0.42

Table 5. Cut-flow for the $4j$ optimization at 13 TeV. EW stands for $(t\bar{t}Wj)_{\rm EW}$.

	$t\bar{t}h$	$W^\pm W^\pm$	$t\bar{t}Z$	$t\bar{t}$-misIDQ	DY-misIDQ	WZ
pre-selection	233	18	105	44	16	41
all cuts	19	3	8	4	0	4

Table 6. Event yields for the subleading backgrounds at 13 TeV, after $4j$ pre-selection and after the full $4j$ analysis.

4.3.2 $3j$ analysis

In the $3j$ analysis, we conservatively do not make use of the forward jet that characterizes the signal, and only impose selection cuts on central jets. The pre-selection is identical to the 8 TeV analysis, except that no requirement on H_T is applied. As in the $4j$ analysis, after the pre-selection we perform a cut optimization taking the point $(\Delta_L, \Delta_R) = (0, 1)$ as signal benchmark, using the statistical significance defined in eq. (4.3). The most effective variables in enhancing the significance are found to be $p_T^{\ell_1}, m_{\ell_1\ell_2}$, the MET and S_T. The cut-flow for the optimal cuts is in table 7. After all cuts, we find a significance of 3.0 and a signal to background ratio of ~ 0.2, to be compared with 3.5 and ~ 0.4, respectively, for the $4j$ analysis. The event yields for the subleading backgrounds are reported in table 8. The DY-mis$Q$ background is very strongly suppressed by the MET cut. The signal yields after all cuts are found to be

$$N_{(t\bar{t}Wj)_{\rm EW}}(\Delta_L, \Delta_R) = 27.1 + 21.1\,\Delta_L + 240.2\,\Delta_L^2 + 3.2\,\Delta_R + 50.4\,\Delta_L\Delta_R + 58.0\,\Delta_R^2 \quad (4.4)$$

$$N_{(t\bar{t}Wj)_{\rm EW}}(\bar{c}_L, \bar{c}_R) = 27.1 - 98.4\,\bar{c}_L + 190.4\,\bar{c}_L^2 - 251.2\,\bar{c}_L^3 + 597.2\,\bar{c}_L^4 + 6.5\,\bar{c}_R - 0.5\,\bar{c}_L\bar{c}_R - 202.6\,\bar{c}_L^2\bar{c}_R + 591.2\,\bar{c}_R^2\,. \quad (4.5)$$

The statistical uncertainty on the signal yields computed using eqs. (4.4) and (4.5) is approximately 10%. To set constraints on the parameters $\vec{p}$ we follow exactly the same procedure described for the $4j$ analysis, including taking into account the contamination due to the $t\bar{t}Z$ process. The resulting bounds are shown as green contours in figure 8.[13] If

[13] From figure 8 we read that, in the absence of systematics on the background, the $3j$ analysis gives a stronger constraint than the $4j$ one in the $\Delta_L = 0\,,\ \Delta_R > 0$ direction. This may be surprising, considering

JHEP01(2016)071

	$\mathcal{S}$	EW(SM)	EW($\Delta_R = 1$)	$(t\bar{t}W$+jets$)_{\rm QCD}$	misIDℓ	S/B
pre-selection	2.5	108	212	678	788	0.066
$p_T^{\ell_1} > 100\,\text{GeV}$	2.9	52	129	346	258	0.12
$m_{\ell_1\ell_2} > 125\,\text{GeV}$	2.9	45	117	308	170	0.14
MET $> 50\,\text{GeV}$	3.0	32	96	229	122	0.17
$S_T > 500\,\text{GeV}$	3.0	25	82	186	80	0.19

Table 7. Cut-flow for the $3j$ optimization at 13 TeV. EW stands for $(t\bar{t}Wj)_{\rm EW}$.

	$t\bar{t}h$	$W^\pm W^\pm$	$t\bar{t}Z$	$t\bar{t}$-misIDQ	DY-misIDQ	WZ
pre-selection	324	32	188	81	32	62
all cuts	35	12	36	10	0	16

Table 8. Event yields for the subleading backgrounds at 13 TeV, after $3j$ pre-selection and after the full $3j$ analysis.

we assume that the only deformation of the SM is a modification of the Zt_Rt_R coupling, we find at 95% CL

$$\begin{aligned} &-0.98 < \Delta_R < 0.70 \quad \text{or} \quad -0.31 < \bar{c}_R < 0.22 \quad (\text{no syst on } B), \\ &-1.34 < \Delta_R < 1.05 \quad \text{or} \quad -0.42 < \bar{c}_R < 0.33 \quad (50\% \text{ syst on misID}\ell). \end{aligned} \tag{4.6}$$

We see that in the $3j$ analysis, the deterioration of the bound due to the large systematic uncertainty on the misIDℓ background is stronger than in the $4j$ analysis, where this background is more effectively suppressed by the cuts.

4.4 Perturbative unitarity of the hard scattering process

As we discussed at length, the growth with the square of the energy of the $tW \to tW$ scattering amplitude is the reason behind the sensitivity of our analysis to anomalous top-Z couplings. However, this growth also implies that at sufficiently high energy, the amplitude becomes so large that perturbative unitarity is lost, making our predictions not trustable. The scale at which this takes place can be estimated, for example, by computing the s-wave amplitude

$$a_0 = \frac{1}{16\pi s}\int_{-s}^{0} dt\mathcal{M}\,, \tag{4.7}$$

where $\mathcal{M}$ is the amplitude, and requiring that $|a_0| < 1$.[14] Considering first deviations in the Zt_Rt_R coupling, by integration of the $\mathcal{M}_{RR}$ amplitude in eqs. (3.1), (3.2), one finds

that we chose this very direction for the optimization of the cuts, and that the $4j$ analysis reached a higher significance (3.5 versus 3.0). The effect is due to the $t\bar{t}Z$ contamination, which slightly shifts all contours, and does so more markedly for the $3j$ analysis, where the $t\bar{t}Z$ contribution to the signal region is larger.

[14] With this definition, perturbative unitarity in WW scattering is lost, in the absence of a Higgs boson, at the scale $\Lambda = 4\sqrt{2\pi}\,v \simeq 2.5\,\text{TeV}$.

JHEP01(2016)071

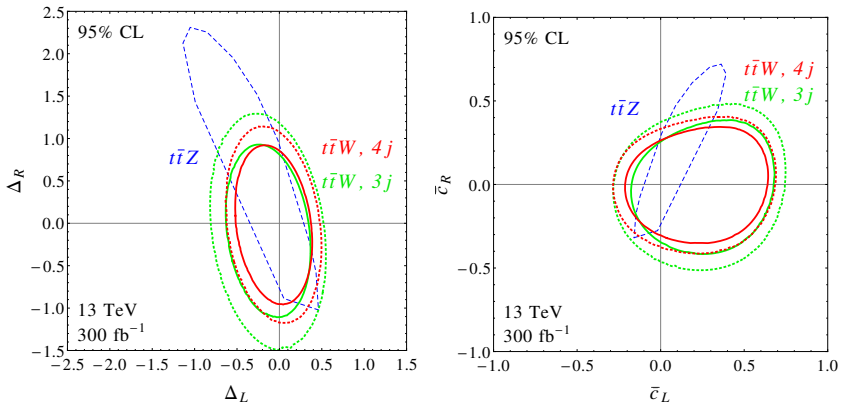

Figure 8. In green, the constraints on top-Z coupling deviations (left panel) and HDO coefficients (right panel) derived from our $3j$ $t\bar{t}W$ analysis at 13 TeV. The solid contour assumes no systematic uncertainty on the background, whereas the dotted one includes a 50% systematic on the misIDℓ component. For comparison, in red we show the corresponding constraints derived from the $4j$ $t\bar{t}W$ analysis, and in dashed blue the constraint obtained from the 13 TeV $t\bar{t}Z$ analysis, as derived in ref. [6]. The red and blue contours are identical to figure 5.

the following estimate for the cutoff scale

$$\Lambda = \frac{3\sqrt{\pi}\, v}{s_w \sqrt{|\Delta_R|}}\,, \tag{4.8}$$

which equals 2.7 TeV for $|\Delta_R| = 1$, corresponding to a BSM contribution of the same size of the SM coupling. Similarly, for deviations in the Zt_Lt_L coupling the relevant amplitude is $\mathcal{M}_{LL}$, leading to

$$\Lambda = \frac{2\sqrt{3\pi}\, v}{\sqrt{1-\frac{4}{3}s_w^2}\,\sqrt{|\Delta_L|}}\,, \tag{4.9}$$

which equals 1.8 TeV for $|\Delta_L| = 1$. To understand whether perturbative unitarity is an issue in our signal predictions, we should consider the distribution of the center-of-mass energy $\sqrt{\hat{s}}$ of the partonic hard scattering $tW \to tW$ in LHC events. However, given the topology of the signal process $pp \to t\bar{t}Wj$, it is impossible to tell on an event-by-event basis whether the hard scattering that took place was $tW \to tW$, or rather $\bar{t}W \to \bar{t}W$. Thus, to be conservative, for each event we identify $\sqrt{\hat{s}}$ with the largest of the partonic invariant masses $m(tW)$ and $m(\bar{t}W)$. Normalized distributions of this quantity are shown in figure 9. For each collider energy we show the distributions, obtained after all selection cuts, for a set of signal points that sit approximately at the edge of the exclusion region, together with the corresponding cutoff scales obtained from eqs. (4.8) and (4.9). We observe that even for the very large deviations allowed by 8 TeV data, the fraction of events whose $\sqrt{\hat{s}}$ could potentially be larger than the cutoff is at most 10%. At 13 TeV, this fraction is approximately 1%. We conclude that our predictions are robustly safe from issues with perturbative unitarity.

JHEP01(2016)071

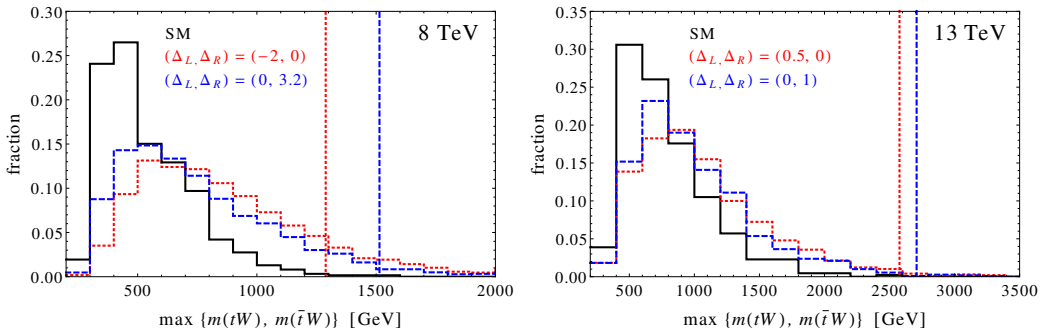

Figure 9. Distributions of the partonic center of mass energy, defined as the largest between $m(tW)$ and $m(\bar{t}W)$, for $(t\bar{t}Wj)_{\rm EW}$ signal events at 8 TeV (left panel) and 13 TeV (right panel). The distributions, shown for a set of representative signal points and for the SM, are obtained after application of all selection cuts. The cutoff scales corresponding to each signal point are also shown as vertical lines.

5 Other processes

In this section we wish to discuss other scattering processes beyond $tW \to tW$ that involve third generation fermions and W, Z or h, where BSM deviations lead to a growth with energy. We will focus on the phenomenologically most relevant amplitudes, pointing out the deformations of the SM to which they are most sensitive to, as well as the most promising collider processes where they could be probed. While our formulas for the amplitudes are expressed in terms of general coupling deviations, in the discussion we assume that departures from the SM can be parameterized in terms of dim-6 operators, including those proportional to $-\bar{c}_L^{(3)} = \bar{c}_L^{(1)} \equiv \bar{c}_L$, $\bar{c}_R$, and $\bar{c}_u$, and neglecting the remaining ones in eq. (2.5). The relation between the HDO coefficients and the coupling deviations can be found in eqs. (2.6)–(2.8). For all processes of the type $\psi_1 + \phi_1 \to \psi_2 + \phi_2$, with $\psi_{1,2} = \{t, b\}$ and $\phi_{1,2}$ the longitudinal $W^\pm, Z$ or h, we make reference to the general form of the amplitude in eq. (3.1).

5.1 $tZ \to th$

For $tZ \to th$ we find $\kappa = 1$ and

$$\begin{aligned} A_{LL} &= c_L^h \left(1 - \frac{4}{3} s_w^2\right), \\ A_{RR} &= -c_R^h \frac{4}{3} s_w^2, \\ A_{LR} &= c_L^h + \frac{1}{2} c_L (c_t - c_V) - \frac{2}{3} s_w^2 \left[2c_L^h + (c_L - c_R)(c_t - c_V)\right], \\ A_{RL} &= -\frac{1}{2} c_L (c_t - c_V) - \frac{2}{3} s_w^2 \left[2c_R^h - (c_L - c_R)(c_t - c_V)\right]. \end{aligned} \tag{5.1}$$

This process can be probed in $pp \to t\bar{t}hj$. The leading terms of the amplitude grow as $\hat{s}$ and are controlled by the $hZtt$ interaction, which under our assumptions receives contributions

JHEP01(2016)071

from both $\bar{c}_L$ and $\bar{c}_R$: we have $A_{LL} \sim \bar{c}_L$ and $A_{RR} \sim \bar{c}_R$. As a consequence, $tZ \to th$ can be seen as complementary to $tW \to tW$ in probing these two operators, and in particular $\bar{c}_R$. However, one important difference between the $t\bar{t}Wj$ and $t\bar{t}hj$ processes is that for the former the $(t\bar{t}W+\text{jets})_{\text{QCD}}$ background is robustly insensitive to new physics in the top sector, whereas for the latter the main background is given by $t\bar{t}h$+jets production, which depends strongly on $c_t = 1 - \bar{c}_u$. The $t\bar{t}h$ signal has been searched for both by ATLAS [39–41] and CMS [42], with 8 TeV data implying an upper limit on the cross section of about 3 times the SM prediction. To enhance the sensitivity to $\bar{c}_L$ and $\bar{c}_R$, one may add to the existing experimental strategy the requirement of a forward jet, as well as additional high energy cuts on the decay products of the Higgs and the tops. It is interesting to note that if an excess were found in $t\bar{t}h$+jets, in principle this could be caused either by $c_t > 1$, or by a large deviation of the Zt_Rt_R coupling.

5.2 $bW \to th$

For $bW^+ \to th$ we find $\kappa = \sqrt{2}$ and

$$\begin{aligned} A_{LL} &= c^h_{LL}\,, \\ A_{RR} &= c^h_{RR}\,, \\ A_{LR} &= c^h_{LL} + \frac{1}{2} c_{LL}(c_t - c_V), \\ A_{RL} &= c^h_{RR} + \frac{1}{2} c_{RR}(c_t - c_V). \end{aligned} \tag{5.2}$$

This process can be probed in $pp \to thj$. The leading terms of the amplitude grow as $\hat{s}$ and are controlled by the $hWtb$ interaction, which under our assumptions is generated only by the operator proportional to $\bar{c}_L$: we have $A_{LL} = -\bar{c}_L$ and $A_{RR} = 0$, thus the leading sensitivity is to $\bar{c}_L$. An interesting feature of the $bW \to th$ process is that the SM amplitude is strongly suppressed, due to an accidental cancellation between the diagrams with s-channel top exchange and t-channel W exchange [18]. As pointed out in refs. [16, 17] (see also ref. [63]), if only Higgs coupling deviations are considered, this cancellation leads to a striking sensitivity of the cross section to $A_{LR} \sim (c_t - c_V)$, which can be exploited to constrain the sign of c_t through a measurement of the thj process. Following this proposal, the CMS collaboration has performed a full analysis on 8 TeV data [64], considering the Higgs decays into $b\bar{b}$, multileptons and $\gamma\gamma$, whereas the ATLAS collaboration has published an analysis in the diphoton channel [39]. We stress that the very strong sensitivity of thj to $(c_t - c_V)$ is mainly due to the threshold region, because of the already mentioned accidental cancellation, thus justifying why the cross section increases by more than one order of magnitude for $c_t = -c_V = -1$, even though the amplitude only grows as $\sqrt{\hat{s}}$ [17]. For more details on the experimental strategy to separate the thj signal from the background, we refer the reader to the analyses in ref. [64]. Here we simply observe that the growth of the amplitude like $\hat{s}$ in the presence of a non-vanishing $\bar{c}_L$ suggests the application of tighter cuts on the Higgs and top decay products. In summary, thj may provide an interesting opportunity to constrain $\bar{c}_L$.

JHEP01(2016)071

5.3 $bW \to tZ$

For $bW^+ \to tZ$ we have $\kappa = 1/\sqrt{2}$ and

$$\begin{aligned} A_{LL} &= c_{LL}\left[2 - c_L - c_{L^b} + \frac{2}{3}s_w^2(2c_L + c_{L^b} - 3)\right], \\ A_{RR} &= c_{RR}\left[2 + \frac{2}{3}s_w^2(2c_R + c_{R^b} - 3)\right], \\ A_{LR} &= c_{LL}\left[1 - c_{L^b} + \frac{2}{3}s_w^2(2c_R + c_{L^b} - 3)\right], \\ A_{RL} &= c_{RR}\left[1 - c_L + \frac{2}{3}s_w^2(2c_L + c_{R^b} - 3)\right]. \end{aligned} \tag{5.3}$$

This scattering can be probed at the LHC through $pp \to tZj$, which was already suggested in refs. [6, 65] as a probe of the top-Z couplings. For the pieces that grow like $\hat{s}$ we find $A_{LL} = 2\bar{c}_L(1 - \bar{c}_L)$ and $A_{RR} = 0$, thus the leading sensitivity is to the coefficient $\bar{c}_L$. In figure 10 we show the partonic cross section for $Wb \to tZ$ scattering. We observe that the cross section is significantly affected by a non-vanishing $\bar{c}_L$, not only at large $\sqrt{\hat{s}}$ but also in the threshold region. On the contrary, $\bar{c}_R$ has a very small impact on the cross section, because its effect arises via the subleading amplitude proportional to $A_{LR} = \bar{c}_R(1 - \bar{c}_L)$, which grows only like $\sqrt{\hat{s}}$. In the SM, the cross section for tZ production at the LHC is almost as large as the one for $t\bar{t}Z$, despite the fact that the former is a b-initiated pure electroweak process [65]. This is due to the lower number of particles in the final state and the lower mass threshold. Notice that tZj gives rise to the trilepton final state, therefore in principle it could be picked up by the CMS 8 TeV $t\bar{t}Z$ search in the trilepton final state of ref. [19]. However, the CMS event selection required at least four jets, among which at least two must be b-tagged, thus strongly suppressing the tZj contribution. In fact, in ref. [65] jet multiplicity was studied as a potential handle to distinguish tZ from $t\bar{t}Z$ production. Based on these preliminary considerations, we conclude that tZ production has negligible sensitivity to $\bar{c}_R$, but may provide another opportunity to constrain the coefficient $\bar{c}_L$.

5.4 $tZ \to tZ$

Next we consider $tZ \to tZ$. We find $\kappa = 1/2$ and

$$\begin{aligned} A_{LL} &= A_{RR} = 0\,, \\ A_{LR} &= A_{RL} = (c_L^2 - c_t c_V) - \frac{8}{3}s_w^2 c_L(c_L - c_R) + \frac{16}{9}s_w^4(c_L - c_R)^2\,. \end{aligned} \tag{5.4}$$

This process can be probed in $pp \to t\bar{t}Zj$. Differently from $tW \to tW$, however, the $tZ \to tZ$ amplitude grows only linearly with energy, the corresponding coefficients $A_{LR} = A_{RL}$ depending on a combination of $\bar{c}_L, \bar{c}_R$ and $\bar{c}_u$. As explained in section 2, the absence of the $\hat{s}/v^2$ growth is a consequence of the symmetry structure of the $\chi\partial\chi\bar{\psi}\gamma\psi$ interactions. The sensitivity to $\bar{c}_u$ is especially interesting, because it is absent in the dominant process for $t\bar{t}Z$ production, which is of $O(g_s^2 g_w)$ and only depends on $\bar{c}_L, \bar{c}_R$. Thus the $t\bar{t}Zj$ final state may in principle provide new information on $\bar{c}_u$. The experimental strategy would rely on

JHEP01(2016)071

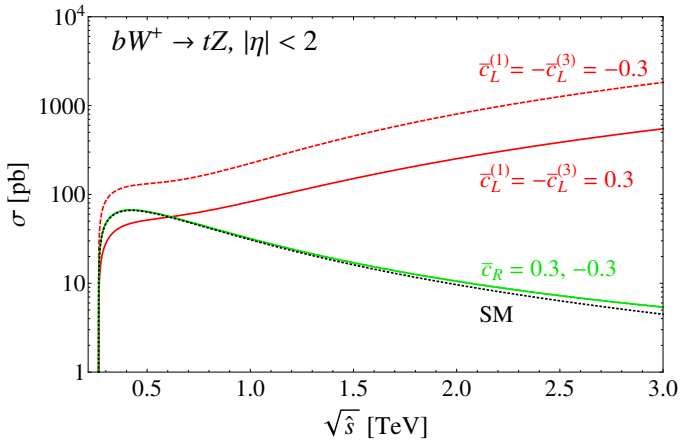

Figure 10. Partonic cross section for the process $bW^+ \to tZ$ as a function of the center of mass energy $\sqrt{\hat{s}}$. A pseudorapidity cut $|\eta| < 2$ has been applied to remove the contribution of the forward region, which is enhanced by the diagram with W exchange in the t-channel. At large energy, the red curves diverge like $\hat{s}$, the green curves (which are indistinguishable) tend to a constant limit, whereas the SM cross section (blue) falls off as $1/\hat{s}$.

the trilepton final state, and the sensitivity to the $O(g_s g_w^3)$ contribution may be enhanced through a forward jet cut. Furthermore, since the amplitude grows with energy, a more stringent cut on the p_T of the Z could also be effective.

5.5 $t\bar{t} \to hh$

The last process we consider is $t\bar{t} \to hh$. The pieces of the amplitude that grow with energy can be written as[15]

$$\begin{pmatrix} \mathcal{M}_{LL} & \mathcal{M}_{RL} \\ \mathcal{M}_{LR} & \mathcal{M}_{RR} \end{pmatrix} = -\frac{g^2}{m_W^2} c_t^h m_t \sqrt{\hat{s}} \begin{pmatrix} 0 & 1 \\ -1 & 0 \end{pmatrix} , \tag{5.5}$$

where to make the notation uniform with eq. (3.1), in $\mathcal{M}_{ij}$ the index i indicates the chirality of the top, and the index j indicates the opposite of the chirality of the antitop. This process can be probed in $pp \to t\bar{t}hh$, which was studies in detail in ref. [66], with an emphasis on its potential role in constraining the Higgs cubic coupling. Based on the form of the amplitude in eq. (5.5), we observe that the main sensitivity of the cross section is not to deviations in the Higgs cubic coupling, which do not lead to a growth of the amplitude with energy, but to the $h^2 t\bar{t}$ contact interaction (in turn proportional to $\bar{c}_u$), which leads to a growth like $m_t\sqrt{\hat{s}}/v^2$ of the amplitude. This conclusion is familiar from studies of the loop-induced process $gg \to hh$, which gives the largest contribution to the double Higgs production rate at the LHC and was shown to be strongly enhanced in presence of a $t\bar{t}hh$ interaction [67]. In fact, the $t\bar{t} \to hh$ amplitude can be obtained by performing an s-channel cut of $gg \to hh$. While $\bar{c}_u$ will be constrained within 15% by $t\bar{t}h$ production at LHC Run-2 [3], due to the growth of the amplitude with energy the residual effect in $pp \to t\bar{t}hh$ may be non-negligible, and potentially affect the Higgs cubic coupling constraint.

[15] Here we define $\hat{s} = (p_t + p_{\bar{t}})^2$.

JHEP01(2016)071

6 Conclusions

Progress towards an understanding of the weak scale requires testing the properties of the top quark. In natural models of electroweak symmetry breaking, the couplings of the latter generically deviate from their SM values. As long as the top couples strongly to the new physics resonances, such deformations can be large without requiring new light states. Examples of resonances are heavy vector bosons or vector-like fermions, typical of models where the Higgs arises from a strongly-interacting sector.

In this paper we proposed a new approach to measure deviations in the top electroweak couplings, which exploits the growth with energy of certain scattering amplitudes involving tops and longitudinal gauge bosons or Higgses. This high energy behaviour can be efficiently probed at the LHC, thanks to the large center of mass energies available. As a proof of concept, we studied in detail $tW \to tW$ scattering, which diverges with the square of the energy in the presence of non-standard ttZ couplings and can be studied at the LHC in $t\bar{t}Wj$ production. By recasting an 8 TeV CMS search for $t\bar{t}W$ in the same-sign lepton final state [19], we extracted constraints on the top-Z couplings. We obtain improved limits compared to those derived from the "conventional" measurement of $t\bar{t}Z$ production, even though the analysis of ref. [19] was not optimized for our signal. For example, considering only a deviation in the Zt_Rt_R coupling we find $-3.6 < \Delta_R < 2.4$ at 95% CL.

Having verified the effectiveness of our method, we proposed a dedicated 13 TeV analysis. We exploited the distinctive kinematic properties of the $t\bar{t}Wj$ signal, namely a tW pair with large invariant mass and a highly energetic forward jet, to suppress the background, mainly composed by $(t\bar{t}W\text{+jets})_{\text{QCD}}$ and misIDℓ. Assuming 300 fb^{-1} of integrated luminosity and no systematic uncertainty on the background, we find $-0.83 < \Delta_R < 0.74$ at 95% CL. In terms of the unique dim-6 operator that modifies the Zt_Rt_R coupling, this reads $-0.26 < \bar{c}_R < 0.23$. In the context of composite Higgs models with a fully composite t_R, where $\bar{c}_R \sim v^2/f^2$ with f the Goldstone-Higgs decay constant, the bound translates into $f \gtrsim 500$ GeV.

In addition, we identified several other amplitudes in the same class that could provide further evidence of the strong connection of the top quark with the new physics sector responsible for electroweak symmetry breaking. An interesting example is the $tZ \to th$ process, which is sensitive to modifications of Zt_Rt_R and can be probed at the LHC in $t\bar{t}hj$ production. It follows that $t\bar{t}h$+jets is sensitive to both of the two least known top couplings, namely Zt_Rt_R and htt, making it an ideal place to look for signs of BSM physics. This warrants further work, to fully exploit the opportunities offered by the LHC in testing the top-Higgs sector.

Acknowledgments

We have benefited from discussions with F. Maltoni. We thank B. Mangano and A. Brinkerhoff for correspondence about refs. [19] and [44], respectively, and D. Curtin and Y. Tsai for discussions about the fake lepton simulation. JD and ES are very grateful to V. Hirschi and O. Mattelaer for their help with MadGraph5_aMC@NLO. ES wishes to thank R. Röntsch

JHEP01(2016)071

for correspondence about a typo in v1 of ref. [6], which was eventually corrected in v2. The work of JD and MF is partly supported by the NSF through grant PHY-1316222. JD is supported in part by the NSERC Grant PGSD3-438393-2013, and MF by the DOE Grant DE-SC0003883. ES is supported by the DOE under Grant DE-SC-000999. JS has been supported in part by the MIUR-FIRB Grant RBFR12H1MW and the ERC Advanced Grant no. 267985 (*DaMeSyFla*). MF, ES and JS thank for hospitality and partial support (1) the Galileo Galilei Institute for Theoretical Physics, where this project was initiated, and (2) the Munich Institute for Astro- and Particle Physics of the DFG cluster of excellence "Origin and Structure of the Universe", where part of the work was done.

JHEP01(2016)071

A Electroweak chiral Lagrangian

In the custodial invariant electroweak chiral Lagrangian the $\mathrm{SU}(2)_L \times \mathrm{U}(1)_Y$ SM gauge symmetry is non-linearly realized, with the Nambu-Goldstone bosons eaten by the W and Z parameterized by the 2×2 matrix

$$\Sigma(x) = \exp\left(i\sigma^a \chi^a(x)/v\right) , \tag{A.1}$$

where σ^a are the Pauli matrices. Such a Σ field describes the spontaneous breaking $\mathrm{SU}(2)_L \times \mathrm{SU}(2)_R \to \mathrm{SU}(2)_V$, with $\mathrm{U}(1)_Y \subset \mathrm{SU}(2)_R$. The Higgs boson h is introduced as a singlet under the custodial $\mathrm{SU}(2)_V$ symmetry.

The interactions of the top (and bottom) are given, at the level of one derivative, by

$$\begin{aligned}
\mathcal{L}_t^{\chi} = {} & i\bar{q}_L \gamma^\mu D_\mu q_L + i\bar{t}_R \gamma^\mu D_\mu t_R + i\bar{b}_R \gamma^\mu D_\mu b_R \\
& - \frac{y_t v}{\sqrt{2}} \bar{q}_L \Sigma P_u t_R \left(1 + \hat{c}_t \frac{h}{v} + 2\hat{c}_t^h \frac{h^2}{v^2} + \cdots\right) + \text{h.c.} \\
& - \frac{i}{2}\mathrm{Tr}\left[\sigma^3 \Sigma^\dagger D_\mu \Sigma\right] \bar{q}_L \gamma^\mu q_L \left(\hat{c}_{L^{(1)}} + 2\hat{c}^h_{L^{(1)}} \frac{h}{v} + \cdots\right) \\
& + \frac{i}{2}\mathrm{Tr}\left[\sigma^3 \Sigma^\dagger D_\mu \Sigma\right] \bar{q}_L \gamma^\mu \Sigma \sigma^3 \Sigma^\dagger q_L \left(\hat{c}_{L^{(2)}} + 2\hat{c}^h_{L^{(2)}} \frac{h}{v} + \cdots\right) \\
& + \frac{i}{2}\mathrm{Tr}\left[\Sigma^\dagger \sigma^a D_\mu \Sigma\right] \bar{q}_L \gamma^\mu \sigma^a q_L \left(\hat{c}_{L^{(3)}} + 2\hat{c}^h_{L^{(3)}} \frac{h}{v} + \cdots\right) \\
& - \frac{i}{2}\mathrm{Tr}\left[\sigma^3 \Sigma^\dagger D_\mu \Sigma\right] \bar{t}_R \gamma^\mu t_R \left(\hat{c}_R + 2\hat{c}^h_R \frac{h}{v} + \cdots\right) \\
& - \frac{i}{2}\mathrm{Tr}\left[\sigma^3 \Sigma^\dagger D_\mu \Sigma\right] \bar{b}_R \gamma^\mu b_R \left(\hat{c}_{R^b} + 2\hat{c}^h_{R^b} \frac{h}{v} + \cdots\right) \\
& + i P_u^T \Sigma^\dagger D_\mu \Sigma P_d \, \bar{t}_R \gamma^\mu b_R \left(\hat{c}_{R^{tb}} + 2\hat{c}^h_{R^{tb}} \frac{h}{v} + \cdots\right) + \text{h.c.} ,
\end{aligned} \tag{A.2}$$

where the dots stand for higher order h interactions. In eq. (A.2) we introduced $P_u = (1,0)^T$, $P_d = (0,1)^T$ as projectors onto the $Y = -1/2, +1/2$ components of Σ respectively,

and $D_\mu\Sigma = \partial_\mu\Sigma - igW^a_\mu\sigma^a\Sigma/2 + ig'B_\mu\Sigma\sigma^3/2$. From eq. (A.1) one finds,

$$\begin{aligned}
-\frac{i}{2}\mathrm{Tr}\left[\sigma^3\Sigma^\dagger D_\mu\Sigma\right] &\overset{\Sigma=1}{=} -\frac{g}{2c_w}Z_\mu\,,\\
+\frac{i}{2}\mathrm{Tr}\left[\Sigma^\dagger\sigma^a D_\mu\Sigma\right] &\overset{\Sigma=1}{=} \frac{g}{2}W^a_\mu - \frac{g'}{2}B_\mu\delta^{a3}\,,\\
iP_u^T\Sigma^\dagger D_\mu\Sigma P_d &\overset{\Sigma=1}{=} \frac{g}{\sqrt{2}}W^+_\mu\,,
\end{aligned} \tag{A.3}$$

in the unitary gauge $\Sigma = 1$, or equivalently at the leading order in the Nambu-Goldstone bosons χ^a. The relations between the coefficients in eq. (2.1) and those in eq. (A.2) trivially follow,

$$\begin{aligned}
&c_L = 1 + \frac{-\hat{c}_{L^{(1)}} + \hat{c}_{L^{(2)}} + \hat{c}_{L^{(3)}}}{1-\frac{4}{3}s_w^2}\,, \qquad c_{L^b} = 1 + \frac{\hat{c}_{L^{(1)}} + \hat{c}_{L^{(2)}} + \hat{c}_{L^{(3)}}}{1-\frac{2}{3}s_w^2}\,, \qquad c_{LL} = 1 + \hat{c}_{L^{(3)}}\,,\\
&c_R = 1 + \frac{\hat{c}_R}{\frac{4}{3}s_w^2}\,, \qquad c_{R^b} = 1 - \frac{\hat{c}_{R^b}}{\frac{2}{3}s_w^2}\,, \qquad c_{RR} = \hat{c}_{R^{tb}}\,, \qquad c_t = \hat{c}_t\,,
\end{aligned} \tag{A.4}$$

and similarly for the $\hat{c}^h_i$ coefficients. Better suited to understand the high energy behaviour of scattering amplitudes is the gauge-less limit, $g, g' \to 0$. In that case one finds

$$\begin{aligned}
-\frac{i}{2}\mathrm{Tr}\left[\sigma^3\Sigma^\dagger D_\mu\Sigma\right] &\overset{g,g'\to0}{=} \frac{1}{v}\partial_\mu\chi_3 + \frac{1}{v^2}\left(\chi_1\partial_\mu\chi_2 - \chi_2\partial_\mu\chi_1\right) + O(\chi^3)\,,\\
+\frac{i}{2}\mathrm{Tr}\left[\Sigma^\dagger\sigma^a D_\mu\Sigma\right] &\overset{g,g'\to0}{=} -\frac{1}{v}\partial_\mu\chi_a + \frac{1}{v^2}\epsilon_{abc}\chi_b\partial_\mu\chi_c + O(\chi^3)\,,\\
iP_u^T\Sigma^\dagger D_\mu\Sigma P_d &\overset{g,g'\to0}{=} -\frac{\sqrt{2}}{v}\partial_\mu\chi_+ + i\frac{\sqrt{2}}{v^2}\left(\chi_3\partial_\mu\chi_+ - \chi_+\partial_\mu\chi_3\right) + O(\chi^3)\,.
\end{aligned} \tag{A.5}$$

In a similar fashion one can write the leading interactions of the Higgs boson, at the level of two derivatives,

$$\mathcal{L}^\chi_h = \frac{1}{2}(\partial_\mu h)^2 + \frac{v^2}{4}\mathrm{Tr}[|D_\mu\Sigma|^2]\left(1 + 2\hat{c}_V\frac{h}{v} + \cdots\right) - \frac{1}{2}m_h^2h^2 - \hat{c}_3\frac{m_h^2}{2v}h^3 + \cdots\,, \tag{A.6}$$

where the dots stand for higher order h interactions. The relation to eq. (2.3) is given by $c_V = \hat{c}_V$ and $c_3 = \hat{c}_3$.

B Current and projected $t\bar{t}Z$ constraints

Here we discuss briefly the constraints derived from the $t\bar{t}Z$ process, both using 8 TeV data [19] and an existing projection to 13 TeV [6], which we used for comparison with our bounds obtained from $t\bar{t}W$.

B.1 8 TeV $t\bar{t}Z$ bound

The trilepton analysis in ref. [19] was targeted at measuring the $t\bar{t}Z$ process, and thus requires, in addition to two of the leptons being compatible with a Z decay, at least 4 jets, among which at least 2 are b-tagged. To set a limit on the parameters $\vec{p}$ from that analysis,

JHEP01(2016)071

we make use of the event yields listed in table 2 of ref. [19] and we assume a systematic uncertainty of 50% on the total background[16]

$$L(\vec{p}\,;r) = \frac{(N_{S+B})^{N_{\rm obs}} e^{-N_{S+B}}}{N_{\rm obs}!} P_{0.5}(r,1) \tag{B.1}$$

where $P_\sigma(x,x_0)$ was defined in eq. (4.2), and $N_{S+B} = rN_B + \sigma_{t\bar{t}Z}(\vec{p})\mathcal{L}\epsilon$, with $\sigma_{t\bar{t}Z}$ the inclusive cross section for $pp \to t\bar{t}Z$ at 8 TeV, $\mathcal{L} = 19.5$ fb^{-1} the integrated luminosity and ϵ the total efficiency for the SM $t\bar{t}Z$ process. The assumption of constant efficiency is justified, given that the cross section does not grow with energy for non-SM couplings. CMS finds that the contribution of $(t\bar{t}W{+}\text{jets})_{\rm QCD}$ to the signal region is strongly subleading, therefore the sensitivity to the couplings arising from $(t\bar{t}Wj)_{\rm EW}$ is negligible.

B.2 13 TeV $t\bar{t}Z$ projection

The most recent assessment of the projected LHC sensitivity to top-Z couplings in the $pp \to t\bar{t}Z$ process was performed in ref. [6], by making use of a signal computation at NLO in QCD. The authors focused on the trilepton final state, and to set constraints they exploited, in addition to the total cross section, the differential distribution in the azimuthal opening angle between the leptons stemming from the Z decay. Neither backgrounds nor detector effects were considered. To compare with our results we make use of their figure 10, where the relation $\bar{c}_L^{(1)} + \bar{c}_L^{(3)} = 0$ was assumed, and simply map the exclusion contours given there to the planes (Δ_L, Δ_R) and $(\bar{c}_L, \bar{c}_R)$ used in this paper.

C Fake lepton simulation

We follow ref. [48], which proposed a method to efficiently simulate fake leptons starting from MC samples containing jets. The method exploits the relationship between the kinematics of a fake lepton and that of the jet that 'sources' it. It consists in applying to each jet an *efficiency* to generate a fake lepton, assumed to be a function of the jet p_T, and a *transfer function*, which represents a normalized probability distribution for the fraction of the jet p_T that is inherited by the fake lepton. These are parameterized as follows

$$\epsilon_{j\to\ell}(p_T^j) = \epsilon_{200}\left[1 - (1-r_{10})\frac{200 - p_T^j/\text{GeV}}{200-10}\right], \tag{C.1}$$

$$\mathcal{T}_{j\to\ell}(\alpha) = \left(\frac{\sqrt{2\pi}\sigma}{2}\right)^{-1}\left[\text{erf}\left(\frac{1-\mu}{\sqrt{2}\sigma}\right) + \text{erf}\left(\frac{\mu}{\sqrt{2}\sigma}\right)\right]^{-1} e^{-\frac{(\alpha-\mu)^2}{2\sigma^2}}, \tag{C.2}$$

where $\alpha \equiv 1 - p_T^\ell/p_T^j$ is the fraction of the jet momentum that is not transferred to the fake lepton. The residual momentum is assumed to contribute to the MET. The parameter ϵ_{200} represents the efficiency for fake lepton production at $p_T^j = 200$ GeV, whereas r_{10} sets the slope of the efficiency as function of p_T^j. The transfer function is assumed to be a Gaussian

[16] We have verified that by assuming 50% on the total background as the only systematic uncertainty, we reproduce to good accuracy the measurement of the $t\bar{t}Z$ cross section quoted in ref. [19]: we find 197^{+107}_{-97} fb, to be compared with 190^{+108}_{-89} fb.

JHEP01(2016)071

with mean μ and standard deviation σ. In our analysis, the 'source' process is $t\bar{t}$+jets, and we will assume that fake leptons dominantly originate from heavy flavor (b) jets [19]. The parameters of the fake lepton simulation are chosen as follows. We first set, for simplicity, $r_{10} = 1$, which gives an efficiency independent of the jet p_T. We further set $\mu = 0.5$, based on the generic expectation of equal splitting of the momentum between the fake lepton and the neutrino produced in heavy flavor decays. By comparison with the H_T and $p_T^{\ell_1}$ distributions by CMS, which were obtained with a data-driven method and reported in figure 2 of ref. [19], we find that $\sigma = 0.1$ gives reasonable agreement. We are thus left with only one free parameter, the global efficiency, which we fix to $\epsilon_{200} \approx 2.5 \times 10^{-4}$ to reproduce the total event yield of 12.1 quoted by CMS (see table 2). A somewhat similar choice of parameters was made by the authors of ref. [68]. We assume no significant difference occurs between fake lepton production at 8 and 13 TeV, and employ the above values of the parameters in our 13 TeV analysis.

Open Access. This article is distributed under the terms of the Creative Commons Attribution License (CC-BY 4.0), which permits any use, distribution and reproduction in any medium, provided the original author(s) and source are credited.

References

[1] ATLAS collaboration, *Observation of a new particle in the search for the Standard Model Higgs boson with the ATLAS detector at the LHC*, *Phys. Lett.* **B 716** (2012) 1 [arXiv:1207.7214] [INSPIRE].

[2] CMS collaboration, *Observation of a new boson at a mass of 125 GeV with the CMS experiment at the LHC*, *Phys. Lett.* **B 716** (2012) 30 [arXiv:1207.7235] [INSPIRE].

[3] S. Dawson et al., *Working Group Report: Higgs Boson*, arXiv:1310.8361 [INSPIRE].

[4] U. Baur, A. Juste, L.H. Orr and D. Rainwater, *Probing electroweak top quark couplings at hadron colliders*, *Phys. Rev.* **D 71** (2005) 054013 [hep-ph/0412021] [INSPIRE].

[5] E.L. Berger, Q.-H. Cao and I. Low, *Model Independent Constraints Among the Wtb, $Zb\bar{b}$, and $Zt\bar{t}$ Couplings*, *Phys. Rev.* **D 80** (2009) 074020 [arXiv:0907.2191] [INSPIRE].

[6] R. Röntsch and M. Schulze, *Constraining couplings of top quarks to the Z boson in $t\bar{t} + Z$ production at the LHC*, *JHEP* **07** (2014) 091 [*Erratum ibid.* **09** (2015) 132] [arXiv:1404.1005] [INSPIRE].

[7] M.S. Chanowitz and M.K. Gaillard, *The TeV Physics of Strongly Interacting W's and Z's*, *Nucl. Phys.* **B 261** (1985) 379 [INSPIRE].

[8] R. Contino, C. Grojean, M. Moretti, F. Piccinini and R. Rattazzi, *Strong Double Higgs Production at the LHC*, *JHEP* **05** (2010) 089 [arXiv:1002.1011] [INSPIRE].

[9] G.F. Giudice, C. Grojean, A. Pomarol and R. Rattazzi, *The Strongly-Interacting Light Higgs*, *JHEP* **06** (2007) 045 [hep-ph/0703164] [INSPIRE].

[10] B. Bellazzini, C. Csáki and J. Serra, *Composite Higgses*, *Eur. Phys. J.* **C 74** (2014) 2766 [arXiv:1401.2457] [INSPIRE].

[11] G. Panico and A. Wulzer, *The Composite Nambu-Goldstone Higgs*, *Lect. Notes Phys.* **913** (2016) 1 [arXiv:1506.01961] [INSPIRE].

JHEP01(2016)071

[12] B. Lillie, J. Shu and T.M.P. Tait, *Top Compositeness at the Tevatron and LHC*, *JHEP* **04** (2008) 087 [arXiv:0712.3057] [INSPIRE].

[13] A. Pomarol and J. Serra, *Top Quark Compositeness: Feasibility and Implications*, *Phys. Rev.* **D 78** (2008) 074026 [arXiv:0806.3247] [INSPIRE].

[14] K. Kumar, T.M.P. Tait and R. Vega-Morales, *Manifestations of Top Compositeness at Colliders*, *JHEP* **05** (2009) 022 [arXiv:0901.3808] [INSPIRE].

[15] T. Appelquist and M.S. Chanowitz, *Unitarity Bound on the Scale of Fermion Mass Generation*, *Phys. Rev. Lett.* **59** (1987) 2405 [*Erratum ibid.* **60** (1988) 1589] [INSPIRE].

[16] S. Biswas, E. Gabrielli and B. Mele, *Single top and Higgs associated production as a probe of the $Ht\bar{t}$ coupling sign at the LHC*, *JHEP* **01** (2013) 088 [arXiv:1211.0499] [INSPIRE].

[17] M. Farina, C. Grojean, F. Maltoni, E. Salvioni and A. Thamm, *Lifting degeneracies in Higgs couplings using single top production in association with a Higgs boson*, *JHEP* **05** (2013) 022 [arXiv:1211.3736] [INSPIRE].

[18] F. Maltoni, K. Paul, T. Stelzer and S. Willenbrock, *Associated production of Higgs and single top at hadron colliders*, *Phys. Rev.* **D 64** (2001) 094023 [hep-ph/0106293] [INSPIRE].

[19] CMS collaboration, *Measurement of top quark-antiquark pair production in association with a W or Z boson in pp collisions at $\sqrt{s} = 8$ TeV*, *Eur. Phys. J.* **C 74** (2014) 3060 [arXiv:1406.7830] [INSPIRE].

[20] J. Elias-Miro, J.R. Espinosa, E. Massó and A. Pomarol, *Higgs windows to new physics through $D = 6$ operators: constraints and one-loop anomalous dimensions*, *JHEP* **11** (2013) 066 [arXiv:1308.1879] [INSPIRE].

[21] R.D. Peccei and X. Zhang, *Dynamical Symmetry Breaking and Universality Breakdown*, *Nucl. Phys.* **B 337** (1990) 269 [INSPIRE].

[22] E. Malkawi and C.P. Yuan, *A Global analysis of the top quark couplings to gauge bosons*, *Phys. Rev.* **D 50** (1994) 4462 [hep-ph/9405322] [INSPIRE].

[23] R. Alonso, M.B. Gavela, L. Merlo, S. Rigolin and J. Yepes, *Flavor with a light dynamical "Higgs particle"*, *Phys. Rev.* **D 87** (2013) 055019 [arXiv:1212.3307] [INSPIRE].

[24] C. Bernardo et al., *Studying the Wtb vertex structure using recent LHC results*, *Phys. Rev.* **D 90** (2014) 113007 [arXiv:1408.7063] [INSPIRE].

[25] J.F. Kamenik, M. Papucci and A. Weiler, *Constraining the dipole moments of the top quark*, *Phys. Rev.* **D 85** (2012) 071501 [*Erratum ibid.* **D 88** (2013) 039903] [arXiv:1107.3143] [INSPIRE].

[26] ATLAS and CMS collaborations, *Diboson production cross section at LHC*, arXiv:1305.3773 [INSPIRE].

[27] R.S. Gupta, A. Pomarol and F. Riva, *BSM Primary Effects*, *Phys. Rev.* **D 91** (2015) 035001 [arXiv:1405.0181] [INSPIRE].

[28] M. Geller and O. Telem, *Holographic Twin Higgs Model*, *Phys. Rev. Lett.* **114** (2015) 191801 [arXiv:1411.2974] [INSPIRE].

[29] R. Barbieri, D. Greco, R. Rattazzi and A. Wulzer, *The Composite Twin Higgs scenario*, *JHEP* **08** (2015) 161 [arXiv:1501.07803] [INSPIRE].

JHEP01(2016)071

[30] M. Low, A. Tesi and L.-T. Wang, *Twin Higgs mechanism and a composite Higgs boson*, *Phys. Rev.* **D 91** (2015) 095012 [arXiv:1501.07890] [INSPIRE].

[31] B. Batell, S. Gori and L.-T. Wang, *Higgs Couplings and Precision Electroweak Data*, *JHEP* **01** (2013) 139 [arXiv:1209.6382] [INSPIRE].

[32] K. Agashe, R. Contino, L. Da Rold and A. Pomarol, *A Custodial symmetry for $Zb\bar{b}$*, *Phys. Lett.* **B 641** (2006) 62 [hep-ph/0605341] [INSPIRE].

[33] T.M.P. Tait and C.P. Yuan, *Single top quark production as a window to physics beyond the standard model*, *Phys. Rev.* **D 63** (2000) 014018 [hep-ph/0007298] [INSPIRE].

[34] A. Buckley et al., *Global fit of top quark effective theory to data*, *Phys. Rev.* **D 92** (2015) 091501 [arXiv:1506.08845] [INSPIRE].

[35] J. de Blas, M. Chala and J. Santiago, *Renormalization Group Constraints on New Top Interactions from Electroweak Precision Data*, *JHEP* **09** (2015) 189 [arXiv:1507.00757] [INSPIRE].

[36] R. Barbieri, B. Bellazzini, V.S. Rychkov and A. Varagnolo, *The Higgs boson from an extended symmetry*, *Phys. Rev.* **D 76** (2007) 115008 [arXiv:0706.0432] [INSPIRE].

[37] J. Brod, A. Greljo, E. Stamou and P. Uttayarat, *Probing anomalous $t\bar{t}Z$ interactions with rare meson decays*, *JHEP* **02** (2015) 141 [arXiv:1408.0792] [INSPIRE].

[38] ATLAS and CMS collaborations, *Measurements of the Higgs boson production and decay rates and constraints on its couplings from a combined ATLAS and CMS analysis of the LHC pp collision data at $\sqrt{s} = 7$ and 8 TeV*, ATLAS-CONF-2015-044 (2015) [INSPIRE].

[39] ATLAS collaboration, *Search for $H \to \gamma\gamma$ produced in association with top quarks and constraints on the Yukawa coupling between the top quark and the Higgs boson using data taken at 7 TeV and 8 TeV with the ATLAS detector*, *Phys. Lett.* **B 740** (2015) 222 [arXiv:1409.3122] [INSPIRE].

[40] ATLAS collaboration, *Search for the Standard Model Higgs boson produced in association with top quarks and decaying into $b\bar{b}$ in pp collisions at $\sqrt{s} = 8$ TeV with the ATLAS detector*, *Eur. Phys. J.* **C 75** (2015) 349 [arXiv:1503.05066] [INSPIRE].

[41] ATLAS collaboration, *Search for the associated production of the Higgs boson with a top quark pair in multilepton final states with the ATLAS detector*, *Phys. Lett.* **B 749** (2015) 519 [arXiv:1506.05988] [INSPIRE].

[42] CMS collaboration, *Search for the associated production of the Higgs boson with a top-quark pair*, *JHEP* **09** (2014) 087 [*Erratum ibid.* **10** (2014) 106] [arXiv:1408.1682] [INSPIRE].

[43] B. Grinstein, C.W. Murphy, D. Pirtskhalava and P. Uttayarat, *Theoretical Constraints on Additional Higgs Bosons in Light of the 126 GeV Higgs*, *JHEP* **05** (2014) 083 [arXiv:1401.0070] [INSPIRE].

[44] CMS collaboration, *Observation of top quark pairs produced in association with a vector boson in pp collisions at $\sqrt{s} = 8$ TeV*, arXiv:1510.01131 [INSPIRE].

[45] ATLAS collaboration, *Measurement of the $t\bar{t}W$ and $t\bar{t}Z$ production cross sections in pp collisions at $\sqrt{s} = 8$ TeV with the ATLAS detector*, *JHEP* **11** (2015) 172 [arXiv:1509.05276] [INSPIRE].

[46] W. Hollik and D. Pagani, *The electroweak contribution to the top quark forward-backward asymmetry at the Tevatron*, *Phys. Rev.* **D 84** (2011) 093003 [arXiv:1107.2606] [INSPIRE].

JHEP01(2016)071

[47] F. Maltoni, M.L. Mangano, I. Tsinikos and M. Zaro, *Top-quark charge asymmetry and polarization in $t\bar{t}W^{\pm}$ production at the LHC*, *Phys. Lett.* **B 736** (2014) 252 [arXiv:1406.3262] [INSPIRE].

[48] D. Curtin, J. Galloway and J.G. Wacker, *Measuring the $t\bar{t}h$ coupling from same-sign dilepton $+2b$ measurements*, *Phys. Rev.* **D 88** (2013) 093006 [arXiv:1306.5695] [INSPIRE].

[49] J. Alwall et al., *The automated computation of tree-level and next-to-leading order differential cross sections and their matching to parton shower simulations*, *JHEP* **07** (2014) 079 [arXiv:1405.0301] [INSPIRE].

[50] A. Alloul, N.D. Christensen, C. Degrande, C. Duhr and B. Fuks, *FeynRules 2.0 — A complete toolbox for tree-level phenomenology*, *Comput. Phys. Commun.* **185** (2014) 2250 [arXiv:1310.1921] [INSPIRE].

[51] T. Sjöstrand, S. Mrenna and P.Z. Skands, *PYTHIA 6.4 Physics and Manual*, *JHEP* **05** (2006) 026 [hep-ph/0603175] [INSPIRE].

[52] J. Conway, *PGS4*, http://conway.physics.ucdavis.edu/.

[53] R.D. Ball et al., *Parton distributions with LHC data*, *Nucl. Phys.* **B 867** (2013) 244 [arXiv:1207.1303] [INSPIRE].

[54] J. Alwall, S. de Visscher and F. Maltoni, *QCD radiation in the production of heavy colored particles at the LHC*, *JHEP* **02** (2009) 017 [arXiv:0810.5350] [INSPIRE].

[55] F. Maltoni, D. Pagani and I. Tsinikos, *Associated production of a top-quark pair with vector bosons at NLO in QCD: impact on $t\bar{t}H$ searches at the LHC*, arXiv:1507.05640 [INSPIRE].

[56] M. Czakon, P. Fiedler and A. Mitov, *Total Top-Quark Pair-Production Cross Section at Hadron Colliders Through $O(\alpha_S^4)$*, *Phys. Rev. Lett.* **110** (2013) 252004 [arXiv:1303.6254] [INSPIRE].

[57] LHC Higgs Cross Section Working Group, J.R. Andersen et al., *Handbook of LHC Higgs Cross Sections: 3. Higgs Properties*, arXiv:1307.1347 [INSPIRE].

[58] CMS collaboration, *Performance of Electron Reconstruction and Selection with the CMS Detector in Proton-Proton Collisions at $\sqrt{s} = 8$ TeV*, 2015 *JINST* **10** P06005 [arXiv:1502.02701] [INSPIRE].

[59] S. Frixione, V. Hirschi, D. Pagani, H.S. Shao and M. Zaro, *Electroweak and QCD corrections to top-pair hadroproduction in association with heavy bosons*, *JHEP* **06** (2015) 184 [arXiv:1504.03446] [INSPIRE].

[60] M. Aliev, H. Lacker, U. Langenfeld, S. Moch, P. Uwer and M. Wiedermann, *HATHOR: HAdronic Top and Heavy quarks crOss section calculatoR*, *Comput. Phys. Commun.* **182** (2011) 1034 [arXiv:1007.1327] [INSPIRE].

[61] LHC Higgs Cross Section Working Group, https://twiki.cern.ch/twiki/bin/view/LHCPhysics/CERNYellowReportPageAt1314TeV.

[62] M. Backović, T. Flacke, S.J. Lee and G. Perez, *LHC Top Partner Searches Beyond the 2 TeV Mass Region*, *JHEP* **09** (2015) 022 [arXiv:1409.0409] [INSPIRE].

[63] S. Biswas, E. Gabrielli, F. Margaroli and B. Mele, *Direct constraints on the top-Higgs coupling from the 8 TeV LHC data*, *JHEP* **07** (2013) 073 [arXiv:1304.1822] [INSPIRE].

JHEP01(2016)071

[64] CMS collaboration, *Search for the Associated Production of a Higgs Boson with a Single Top Quark in Proton-Proton Collisions at* $\sqrt{s} = 8$ *TeV*, arXiv:1509.08159 [INSPIRE].

[65] J. Campbell, R.K. Ellis and R. Röntsch, *Single top production in association with a Z boson at the LHC*, *Phys. Rev.* **D 87** (2013) 114006 [arXiv:1302.3856] [INSPIRE].

[66] C. Englert, F. Krauss, M. Spannowsky and J. Thompson, *Di-Higgs phenomenology in* $t\bar{t}hh$*: The forgotten channel*, *Phys. Lett.* **B 743** (2015) 93 [arXiv:1409.8074] [INSPIRE].

[67] R. Gröber and M. Mühlleitner, *Composite Higgs Boson Pair Production at the LHC*, *JHEP* **06** (2011) 020 [arXiv:1012.1562] [INSPIRE].

[68] E. Izaguirre and B. Shuve, *Multilepton and Lepton Jet Probes of Sub-Weak-Scale Right-Handed Neutrinos*, *Phys. Rev.* **D 91** (2015) 093010 [arXiv:1504.02470] [INSPIRE].

JHEP01(2016)071